J. Fluid Mech. (2002), *vol.* 465, *pp.* 301–330.
DOI: 10.1017/S0022112002001076 Printed in the United Kingdom

A quasi-steady approach to the instability of time-dependent flows in pipes

By M. S. GHIDAOUI† AND A. A. KOLYSHKIN‡

Department of Civil Engineering, The Hong Kong University of Science & Technology (HKUST), Kowloon, Hong Kong

(Received 6 November 2000 and in revised form 15 March 2002)

Asymptotic solutions for unsteady one-dimensional axisymmetric laminar flow in a pipe subject to rapid deceleration and/or acceleration are derived and their stability investigated using linear and weakly nonlinear analysis. In particular, base flow solutions for unsteady one-dimensional axisymmetric laminar flow in a pipe are derived by the method of matched asymptotic expansions. The solutions are valid for short times and can be successfully applied to the case of an arbitrary (but unidirectional) axisymmetric initial velocity distribution. Excellent agreement between asymptotic and analytical solutions for the case of an instantaneous pipe blockage is found for small time intervals. Linear stability of the base flow solutions obtained from the asymptotic expansions to a three-dimensional perturbation is investigated and the results are used to re-interpret the experimental results of Das & Arakeri (1998). Comparison of the neutral stability curves computed with and without the planar channel assumption shows that this assumption is accurate when the ratio of the unsteady boundary layer thickness to radius (i.e. δ_1/R) is small but becomes unacceptable when this ratio exceeds 0.3. Both the current analysis and the experiments show that the flow instability is non-axisymmetric for $\delta_1/R = 0.55$ and 0.85. In addition, when $\delta_1/R = 0.18$ and 0.39, the neutral stability curves for $n = 0$ and $n = 1$ are found to be close to one another at all times but the most unstable mode in these two cases is the axisymmetric mode. The accuracy of the quasi-steady assumption, employed both in this research and in that of Das & Arakeri (1998), is supported by the fact that the results obtained under this assumption show satisfactory agreement with the experimental features such as type of instability and spacing between vortices. In addition, the computations show that the ratio of the rate of growth of perturbations to the rate of change of the base flow is much larger than 1 for all cases considered, providing further support for the quasi-steady assumption. The neutral stability curves obtained from linear stability analysis suggest that a weakly nonlinear approach can be used in order to study further development of instability. Weakly nonlinear analysis shows that the amplitude of the most unstable mode is governed by the complex Ginzburg–Landau equation which reduces to the Landau equation if the amplitude is a function of time only. The coefficients of the Landau equation are calculated for two cases of the experimental data given by Das & Arakeri (1998). It is shown that the real part of the Landau constant is positive in both cases. Therefore, finite-amplitude equilibrium is possible. These results are in qualitative agreement with experimental data of Das & Arakeri (1998).

† Author to whom correspondence should be addressed.
‡ Permanent address: Department of Engineering Mathematics, Riga Technical University, Riga, Latvia LV 1658.

1. Introduction

The study of unsteady fluid flows in pipes is important for a wide range of applications including the design and analysis of water supply systems and natural gas pipelines and the analysis of blood flow in arteries. Flow unsteadiness in water supply and natural gas pipelines can be triggered by accidental or normal pump shutdowns, pump starts or rapid changes in valve settings and are known to cause rupture of pipelines, damage to other hydraulic devices and fire related damages in the case of natural gas pipelines (Wylie & Streeter 1993). In addition, the pressure in unsteady flow can, during part of the transient cycle, acquire values low enough to cause cavitation, pitting and corrosion, and intrusion of contaminants through cracks and joints (Brunone *et al.* 2000). Water quality in supply lines can be affected following a transient event as bio-film on the pipe is sloughed off by large shear stresses created by the transient and particulates may be re-suspended by the strong mixing of the flow inside a pipe. Moreover, blood flow unsteadiness induced by the cardiac cycle can result in atherosclerosis plaque development in regions where the shear stress changes direction (Waters & Pedley 1999).

The first step in an attempt to describe unsteady flows in pipes is to construct approximate analytical solutions for fluid transients. There are just a few known analytical solutions for unsteady viscous flow motion in a pipe. One classical example is the flow due to constant pressure gradient which is applied instantaneously at $\tilde{t} = 0$. This problem was originally solved by Gromeka (1882) and his solution has been reproduced in many fluid mechanics textbooks (see, for example, Telionis 1981). Weinbaum & Parker (1975) studied the laminar decay of a fully developed channel or pipe flow following a sudden blockage. The velocity distribution was found by the Pohlhausen-type technique used in boundary layer theory. Das & Arakeri (1998) obtained analytical solutions for some unsteady viscous flows in a circular cylinder and plane channel. The flow is generated by the motion of a piston. Das & Arakeri found solutions for the cases where the velocity of piston varies linearly with time (for both accelerating and decelerating flows) or is constant over a certain time interval. These solutions are expressed in terms of infinite series which can be used only if the dimensionless time $\hat{t} = \nu\tilde{t}/R^2$ is not too small, where ν is the viscosity of the fluid, $\tilde{t}$ is time and R is the radius of the pipe. In some applications, however, the parameter $\hat{t}$ can be very small. For example, the time scale of transient flows in water supply systems, natural gas pipelines and blood flow in arteries is of order a few seconds, therefore possible values of $\hat{t}$ are in the range 10^{-6}–10^{-4}. The infinite series obtained by Das & Arakeri (1998) are practically useless in such cases since too many terms of the series must be used in order to obtain the velocity distribution. Ghidaoui & Kolyshkin (2001) investigated the linear stability of flow in a pipe after instantaneous reduction of the flow rate to zero. An approximate analytical solution for the velocity distribution in a pipe was derived by the method of Laplace transform. Note that the method used in Ghidaoui & Kolyshkin (2001) gives closed-form solutions only for some particular cases of the velocity distribution prior deceleration. Hence there is a need to construct approximate analytical solutions for unsteady flows in pipes which can be used for short time intervals.

Previous studies have shown that the velocity profiles in rapidly decelerated flows have inflection points. Hence, these profiles are potentially highly unstable. Therefore, linear stability analysis should be considered as the second natural step in the theoretical description of unsteady flows. When applicable, linear stability analysis provides the starting point for understanding the transition from one flow regime to another in unsteady flows. For example, linear stability analysis of unsteady flows:

(i) delineates the essential parameters governing the transition from one flow regime to another, (ii) points out the most unstable mode and (iii) provides neutral stability curves which are important for nonlinear stability analysis. However, despite its importance, the linear stability of time-dependent flows is a relatively new and not well-developed topic in hydrodynamic stability theory. Drazin & Reid (1981) pointed out that even the terms 'stable flow' and 'unstable flow' may become unclear for the case of time-dependent base flows which change substantially with time. At present, rigorous linear stability analysis of unsteady flows is possible only for periodic base flows, where the Floquet theory can be used (e.g. Yang & Yih 1977; Davis 1976; von Kerczek & Davis 1974).

Shen (1961) performed linear stability analysis of non-periodic flows by assuming that the base flow is separable. However, this assumption does not hold for most unsteady flows. Another approach to the stability analysis of non-periodic unsteady flows is the application of the method of normal modes along with the quasi-steady assumption. This approach has been used in stability studies of pipe entrance flows (Garg 1981; Moss & da Silva 1993; da Silva & Moss 1994), decelerating boundary layers (Gad-el-Hak *et al.* 1984), thermal instability of boundary layers (Krane & Gebhart 1993), non-periodic pipe flows (Das & Arakeri 1998) and waterhammer flows (Ghidaoui & Kolyshkin 2001). The quasi-steady assumption treats time as a parameter and not as an independent variable. Hall & Parker (1976) argued that such an approach is justifiable if there exists a fast (convective) time scale on which a perturbation can grow before significant changes in the base flow can be observed and showed that the quasi-steady approach represents the first term of an asymptotic expansion of the WKB type. In addition, Akhavan, Kamm & Shapiro (1991) stated that the quasi-steady assumption is justified if instability of the Stokes layer is due to the inflection points in the base flow profile. Cowley (1987) pointed out that since the formal justification of the quasi-steady assumption is that the Reynolds number is very large, the viscous terms should be dropped in the analysis. As a result, the instability (to the leading order) is governed by Rayleigh's equation and is essentially inviscid. This consistent approach was used for a stability analysis of sinusoidally oscillating flow above a plane stationary wall with respect to high-frequency disturbances. However, Cowley (1987) pointed out that maintaining the viscous terms can in some cases lead to good results. Indeed, the results of several studies, e.g. Gad-el-Hak *et al.* (1984), Krane & Gebhart (1993), Das & Arakeri (1998) and others indicate that reasonable agreement is found between available experimental results and theoretical data obtained by means of the quasi-steady assumption while maintaining the viscous terms in the stability analysis.

The validity of the quasi-steady assumption can be quantitatively assessed by comparing the growth rates of perturbations with the rate of change of the base flow with respect to time (e.g. as in Krane & Gebhart 1993 and Ghidaoui & Kolyshkin 2001). If the growth rates of perturbations are considerably larger than the rate of change of the base flow, then the quasi-steady approach is justified. Another approach to analyse the quasi-steady approximation is through direct numerical simulation. This approach was used by Yang, Spalart & Ferziger (1992) where they showed that the growth rates calculated by means of the quasi-steady approach in Gad-el-Hak *et al.* (1984) for decelerating boundary layers are in good agreement with the results of direct numerical simulation. However, the results of von Kerczek & Davis (1974) indicate that the quasi-steady approach does not give reasonable results in the case of an oscillatory Stokes layer.

Note that in some cases the critical Reynolds numbers calculated by means of the quasi-steady approach are too low. This is because the smaller the growth rate of disturbance the less accurate is the quasi-steady assumption. The approximation is least accurate at the neutral curve where the growth rate is zero. Gad-el-Hak *et al.* (1984) found that the critical Reynolds numbers calculated by means of the quasi-steady assumption often qualitatively reflect 'the degree of instability' of a particular flow, but in some cases quantitative prediction of transition may be inaccurate.

Recently Das & Arakeri (1998 is referred to herein as DA) performed an experimental study of stability and transition to turbulence of a piston-driven non-periodic flow in a long pipe with circular cross-section. In addition, DA used linear stability theory to analyse the experimental data. Their linear stability analysis was based on the following two assumptions: (i) planar geometry and (ii) the quasi-steady assumption. The theoretical and experimental results are found to be in good qualitative agreement.

In the present paper we: (i) use the method of matched asymptotic expansions to derive unsteady one-dimensional axisymmetric laminar base flow profiles in a pipe subject to rapid deceleration or acceleration, (ii) investigate the stability of these velocity profiles using both linear and weakly nonlinear analysis, (iii) re-interpret the experimental findings of DA on the basis of linear and weakly nonlinear stability results, and (iv) assess the accuracy of the quasi-steady and the planar assumptions used in DA.

2. Asymptotic solution by the method of matched asymptotic expansions

In this section an asymptotic solution for unsteady axisymmetric laminar flow in a pipe is derived by the method of matched asymptotic expansions. Consider an infinitely long horizontal pipe with radius R filled with a viscous incompressible fluid. Starting from time $\tilde{t} = 0$ the flow is accelerated or decelerated so that the total fluid flux through the cross-section of the pipe changes with time. The flow prior to acceleration or deceleration can be either steady or unsteady (but unidirectional). In order to describe the flow we introduce cylindrical polar coordinates $(\tilde{r}, \theta, \tilde{z})$ with the origin on the axis of the pipe. We assume that the velocity vector has only one non-zero component, $\tilde{W}(\tilde{r}, \tilde{t})$, which depends only on the radial position, $\tilde{r}$, and time, $\tilde{t}$. In this case the system of Navier–Stokes equations reduces to the single equation

$$\frac{\partial \tilde{W}}{\partial \tilde{t}} = -\frac{1}{\rho}\frac{\partial \tilde{p}}{\partial \tilde{z}} + \nu\left(\frac{\partial^2 \tilde{W}}{\partial \tilde{r}^2} + \frac{1}{\tilde{r}}\frac{\partial \tilde{W}}{\partial \tilde{r}}\right). \tag{1}$$

The following dimensionless quantities are chosen: time, T, length, R, velocity, U, and pressure, $\rho UR/T$. Here T is the characteristic time over which the acceleration/deceleration is applied, and U is the characteristic velocity. The dimensionless form of equation (1) is

$$\frac{\partial W}{\partial t} = h(t) + \varepsilon\left(\frac{\partial^2 W}{\partial r^2} + \frac{1}{r}\frac{\partial W}{\partial r}\right), \tag{2}$$

where

$$\varepsilon = \frac{\nu T}{R^2} \quad \text{and} \quad h(t) = -\frac{\partial p}{\partial z}.$$

The parameter ε is the ratio of the wave time scale, T, and the diffusion time scale, R^2/ν. In waterhammer applications the value of ε is very small. For example, in the experiments of Holomboe & Roleau (1967) $\varepsilon = 0.0066$ for the laminar case.

Equation (2) is solved with the following boundary and initial conditions

$$W|_{r=1} = 0, \quad W|_{r=0} \text{ is bounded,} \tag{3}$$

$$W|_{t=0} = g(r). \tag{4}$$

The function $g(r)$ represents the velocity distribution prior to acceleration or deceleration. If the flow before the transient starts was steady, then $g(r)$ represents steady velocity distribution (for example, in the case of the Poiseuille flow $g(r) = 1 - r^2$). On the other hand, if the flow before the transient starts was unsteady (but unidirectional), then $g(r)$ represents the velocity distribution across the pipe at that instant (i.e. at $t = 0$). In what follows $g(r)$ is assumed to be an arbitrary smooth function of r which satisfies boundary conditions (3).

The total fluid flux through the cross-section of the pipe for $t \geqslant 0$ is:

$$2\int_0^1 rW(r,t)\,\mathrm{d}r = f(t), \tag{5}$$

where $f(t)$ is a given function of time, t. Applying the Laplace transform to (2)–(5), we obtain

$$s\bar{W} - g(r) = \bar{h} + \varepsilon\left(\frac{\mathrm{d}^2\bar{W}}{\mathrm{d}r^2} + \frac{1}{r}\frac{\mathrm{d}\bar{W}}{\mathrm{d}r}\right), \tag{6}$$

$$\bar{W}|_{r=1} = 0, \quad \bar{W}|_{r=0} \text{ is bounded,} \tag{7}$$

$$2\int_0^1 r\bar{W}(r,s)\,\mathrm{d}r = \bar{f}(s), \tag{8}$$

where s is the parameter of the Laplace transform, and $\bar{W}$, $\bar{h}$ and $\bar{f}$ are the Laplace transforms of the functions W, h and f, respectively.

Since in many applications (for example, in waterhammer) the value of ε is small and since one is often interested in solutions for short times, it is natural to use the methods of perturbation theory (see, for example, Kevorkian & Cole 1996) in order to construct an asymptotic solution to problem (6)–(8). The physical idea behind the perturbation expansion is the following. Suppose that the fluid flux through the cross-section of the pipe is suddenly changed. The sudden change in pressure generates additional vorticity in the region which is infinitely close to the pipe wall. This process is initially inviscid since the change in velocity due to sudden pressure changes does not satisfy the no-slip condition at the wall. After the pressure wave has passed, the additional vorticity starts to diffuse in the radial direction towards the axis of the pipe. As a result of diffusion, a boundary layer starts to develop near the wall. Hence, the velocity distribution in the core region (close to the axis of the pipe) changes slowly while rapid changes are taking place near the wall. The core region is described by the outer part of asymptotic expansion while the boundary layer is represented by the inner expansion. In order to have a balance of viscous and inertia forces near the wall $r = 1$, one should use the following boundary layer variable:

$$\xi = \frac{1-r}{\sqrt{\varepsilon}}. \tag{9}$$

This suggests the following outer expansion for the functions $\bar{W}(r,s)$ and $\bar{h}(s)$:

$$\bar{W}(r,s,\varepsilon) = \bar{W}_0(r,s) + \sqrt{\varepsilon}\,\bar{W}_1(r,s) + \varepsilon\bar{W}_2(r,s) + \cdots, \tag{10}$$

$$\bar{h}(s,\varepsilon) = \bar{h}_0(s) + \sqrt{\varepsilon}\,\bar{h}_1(s) + \varepsilon\bar{h}_2(s) + \cdots \tag{11}$$

Substituting (10) and (11) into (6), (8) and collecting the terms that do not contain ε, we obtain

$$s\bar{W}_0 - g(r) = \bar{h}_0, \tag{12}$$

$$2\int_0^1 r\bar{W}_0(r,s)\,\mathrm{d}r = \bar{f}(s). \tag{13}$$

It follows from (12) and (13) that

$$\bar{W}_0 = \frac{g(r)}{s} - \frac{G}{s} + \bar{f}, \quad \bar{h}_0 = -G + s\bar{f}, \tag{14}$$

where G is the average velocity of undisturbed flow at $t = 0$:

$$G = 2\int_0^1 rg(r)\,\mathrm{d}r. \tag{15}$$

The inner expansion near the wall $r = 1$ is sought in the form

$$\bar{W}(r,s,\varepsilon) = \bar{U}_0(\xi,s) + \sqrt{\varepsilon}\,\bar{U}_1(\xi,s) + \varepsilon\bar{U}_2(\xi,s) + \cdots, \tag{16}$$

where ξ is the boundary layer variable defined by (9). Substituting (16) into (6) and (7) and collecting the terms that do not contain ε, we obtain

$$\frac{\mathrm{d}^2\bar{U}_0}{\mathrm{d}\xi^2} - s\bar{U}_0 = G - s\bar{f}, \tag{17}$$

$$\bar{U}_0|_{\xi=0} = 0. \tag{18}$$

The function $U_0(\xi,t)$ describes the development of the boundary layer near the wall to order unity. Since there was no diffusion at $t = 0$, in order to derive (17) a zero initial condition for U_0 is used. The solution to (17) which satisfies (18) has the form

$$\bar{U}_0(\xi,s) = C_1\,\mathrm{e}^{\sqrt{s}\xi} + \left(\frac{G}{s} - \bar{f}\right)(\mathrm{e}^{-\sqrt{s}\xi} - 1), \tag{19}$$

where C_1 is an arbitrary constant. Using the matching condition

$$\lim_{\xi\to\infty}\bar{U}_0(\xi,s) = \lim_{r\to 1}\bar{W}_0(r,s) \tag{20}$$

we obtain that $C_1 = 0$. It also follows from (20) that

$$\lim_{\xi\to\infty}\bar{U}_0(\xi,s) = \lim_{r\to 1}\bar{W}_0(r,s) = \bar{f} - \frac{G}{s}. \tag{21}$$

A uniformly valid ($0 \leqslant r \leqslant 1$) approximation to order unity is obtained by adding $\bar{W}_0$ and $\bar{U}_0$ and subtracting the common part (21) (see Kevorkian & Cole 1996):

$$\bar{W}(r,s,\varepsilon) = \frac{g(r)}{s} + \bar{f} + \frac{G}{s}(\mathrm{e}^{-\sqrt{s}\xi} - 1) - \bar{f}\,\mathrm{e}^{-\sqrt{s}\xi} + O(\sqrt{\varepsilon}). \tag{22}$$

Note that the function $\bar{W}$ defined by (22) does not satisfy condition (8) (to $O(\sqrt{\varepsilon})$). In fact, substituting (22) into (8) and using (10) we obtain

$$2\int_0^1 r\bar{W}_1(r,s)\,\mathrm{d}r = 2\left(\frac{\bar{f}}{\sqrt{s}} - \frac{G}{s\sqrt{s}}\right). \tag{23}$$

Substituting (10) and (11) into (6) and collecting terms of $O(\sqrt{\varepsilon})$ yields

$$s\bar{W}_1(r,s) = \bar{h}_1(s). \tag{24}$$

Using (23) and (24), we obtain

$$\bar{W}_1(r,s) = \frac{2\bar{f}}{\sqrt{s}} - \frac{2G}{s\sqrt{s}} \quad \text{and} \quad \bar{h}_1(s) = 2\sqrt{s}\,\bar{f} - \frac{2G}{\sqrt{s}}. \tag{25}$$

Substituting (16) into (6) and (7) and collecting the terms of $O(\sqrt{\varepsilon})$ yields

$$\frac{\mathrm{d}^2\bar{U}_1}{\mathrm{d}\xi^2} - s\bar{U}_1 = -2\sqrt{s}\bar{f} + \sqrt{s}\,\bar{f}\,\mathrm{e}^{-\sqrt{s}\xi} + \frac{2G}{\sqrt{s}} - \frac{G}{\sqrt{s}}\,\mathrm{e}^{-\sqrt{s}\xi}, \tag{26}$$

$$\bar{U}_1|_{\xi=0} = 0. \tag{27}$$

Solving (26), (27) and using the matching condition

$$\lim_{\xi\to\infty} \bar{U}_1(\xi,s) = \lim_{r\to 1} \bar{W}_1(r,s), \tag{28}$$

we obtain the function $\bar{U}_1(\xi,s)$ in the form

$$\bar{U}_1(\xi,s) = \left(\frac{2G}{s\sqrt{s}} - \frac{2\bar{f}}{\sqrt{s}}\right)(\mathrm{e}^{-\sqrt{s}\xi} - 1) + \left(\frac{G}{2s} - \frac{\bar{f}}{2}\right)\xi\,\mathrm{e}^{-\sqrt{s}\xi}. \tag{29}$$

Hence, the Laplace transform of the solution up to $O(\varepsilon)$ is

$$\bar{W}(r,s,\varepsilon) = \frac{g(r)}{s} + \left(\frac{G}{s} - \bar{f}\right)(\mathrm{e}^{-\sqrt{s}\xi} - 1) + \sqrt{\varepsilon}\left[\left(\frac{2G}{s\sqrt{s}} - \frac{2\bar{f}}{\sqrt{s}}\right)(\mathrm{e}^{-\sqrt{s}\xi} - 1) + \left(\frac{G}{2s} - \frac{\bar{f}}{2}\right)\xi\,\mathrm{e}^{-\sqrt{s}\xi}\right] + O(\varepsilon). \tag{30}$$

Higher-order terms can be constructed in a similar way. The solution to problem (2)–(5) can be found by inverting the Laplace transform (30) and using the convolution theorem for any given transient scenario which is described by the function $f(t)$.

We present here the solution for one particular case, namely the sudden closure of a pipe. In this case the function $f(t)$ is equal to zero. It is also assumed that the initial velocity distribution before instantaneous deceleration, $g(r)$, corresponds to the case of fully developed Poiseuille flow. The inverse Laplace transform of (30) for the case $f(t) = 0$ and $W|_{t=0} = 1 - r^2$ is

$$W(r,t,\varepsilon) = \tfrac{1}{2} - r^2 + \left(\frac{3r-1}{4}\right)\operatorname{erfc}\left(\frac{1-r}{2\sqrt{\varepsilon t}}\right) + 2\sqrt{\frac{\varepsilon t}{\pi}}\left(\exp\left(-\frac{(1-r)^2}{4\varepsilon t}\right) - 1\right) + O(\varepsilon). \tag{31}$$

Problem (2)–(5) can also be solved analytically by the method of Laplace transform. For an arbitrary function $g(r)$ the solution is given in terms of infinite series whose coefficients contain integrals involving $g(r)$. However, for the case $g(r) = 1 - r^2$ and $f(t) = 0$ the solution to (2)–(5) is

$$W(r,\hat{t}) = \sum_{n=1}^{\infty} \frac{2J_1(\beta_n) - \beta_n J_0(\beta_n r)}{\beta_n^2 J_1(\beta_n)} \exp(-\beta_n^2 \hat{t}), \tag{32}$$

where β_n are the roots of the equation $J_2(\beta) = 0$, $J_m(q)$ is the Bessel function of the first kind of order m and $\hat{t} = v\tilde{t}/R^2$. Note that (32) is written for the case $\varepsilon = 1$, that

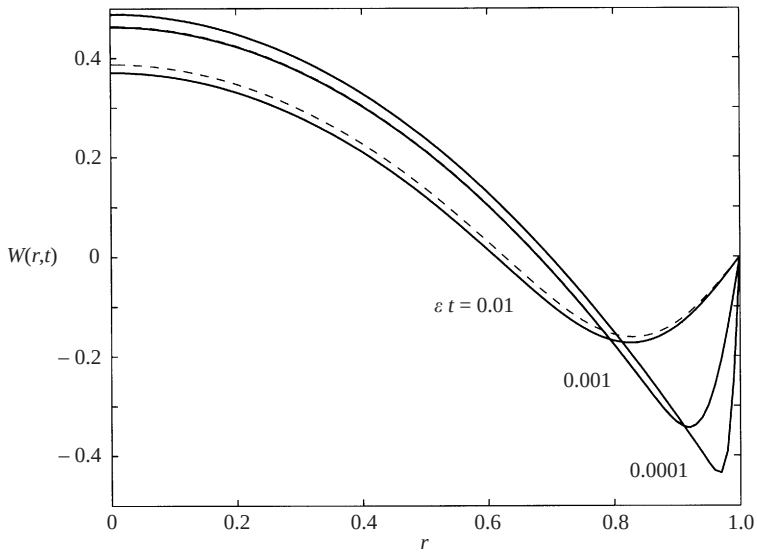

FIGURE 1. Unsteady velocity profiles $W(r,t)$ for different values of $\hat{t} = \varepsilon t$. The solid and dashed lines indicate the exact solution and the asymptotic solution, respectively.

is, where the time scale T is the diffusion time scale R^2/ν. In order to compare the solutions (31) and (32) we simply put $\hat{t} = \varepsilon t$.

Velocity profiles given by formulas (31) and (32) are presented in figure 1 for different values of εt. In order to obtain accurate results for small times, 62 terms of the series (32) are used. It is seen from the figure that as time increases, a boundary layer starts to develop near the wall. The exact solution (32) is shown by solid lines while asymptotic solution (31) is represented by dashed lines. The two solutions for the cases $\varepsilon t = 0.0001$ and $\varepsilon t = 0.001$ are almost indistinguishable. Note that $\varepsilon t = 0.001$ corresponds to the time $\tilde{t} = 10\,\mathrm{s}$ if the radius of the pipe is 10 cm and water is used as the working fluid. A typical transient time in a waterhammer event is, in many cases, less than 10 s. This example shows that the method of matched asymptotic expansions is a powerful tool in analysing rapidly changing unsteady laminar flows in pipes.

3. Formulation of the stability model

Since velocity profiles of decelerated unsteady flows usually contain inflection points (see, for example, figure 1), these profiles are potentially unstable. Therefore it is natural to investigate the conditions under which such flows become linearly unstable. We assume that $u(r,\theta,z,t)$, $v(r,\theta,z,t)$ and $w(r,\theta,z,t)$ denote the radial, azimuthal and longitudinal velocity components, respectively, and $p(r,\theta,z,t)$ represents the pressure. Note that in the remainder of the paper t will denote the dimensionless time scaled with R^2/ν. Consider a perturbed motion of the form

$$\left.\begin{aligned} u(r,z,t) &= u'(r)\,\mathrm{e}^{\mathrm{i}n\theta+\mathrm{i}\alpha z-Re\gamma t},\\ v(r,z,t) &= v'(r)\,\mathrm{e}^{\mathrm{i}n\theta+\mathrm{i}\alpha z-Re\gamma t},\\ w(r,z,t) &= W(r,t)+w'(r)\,\mathrm{e}^{\mathrm{i}n\theta+\mathrm{i}\alpha z-Re\gamma t},\\ p(r,z,t) &= P(t)+p'(r)\,\mathrm{e}^{\mathrm{i}n\theta+\mathrm{i}\alpha z-Re\gamma t}, \end{aligned}\right\} \tag{33}$$

where α is the axial wavenumber, n is the azimuthal wavenumber, u', v', w' and p' are small amplitudes of the normal perturbations, and the Reynolds number is defined by $Re = UR/\nu$, where U is some characteristic velocity scale. Substituting (33) into the Navier–Stokes equations and linearizing the equations in a neighbourhood of the base flow $W(r,t)$, $P(t)$, we obtain the following dimensionless linearized stability equations:

$$-\gamma u' + \mathrm{i}\alpha u' W = -\frac{\mathrm{d}p'}{\mathrm{d}r} + \frac{1}{Re}\left[\mathrm{N}u' - \frac{u'}{r^2} - 2\mathrm{i}n\frac{v'}{r^2}\right], \tag{34}$$

$$-\gamma v' + \mathrm{i}\alpha v' W = -\mathrm{i}n\frac{p'}{r} + \frac{1}{Re}\left[\mathrm{N}v' - \frac{v'}{r^2} + 2\mathrm{i}n\frac{u'}{r^2}\right], \tag{35}$$

$$-\gamma w' + \mathrm{i}\alpha w' W + u'\frac{\partial W}{\partial r} = -\mathrm{i}\alpha p' + \frac{1}{Re}\mathrm{N}w', \tag{36}$$

$$\frac{\mathrm{d}u'}{\mathrm{d}r} + \frac{u'}{r} + \mathrm{i}n\frac{v'}{r} + \mathrm{i}\alpha w' = 0, \tag{37}$$

where

$$\mathrm{N} = \frac{\mathrm{d}^2}{\mathrm{d}r^2} + \frac{1}{r}\frac{\mathrm{d}}{\mathrm{d}r} - \frac{n^2}{r^2} - \alpha^2.$$

Note that the quasi-steady approximation is used in deriving equations (34)–(37), that is the variable t in $W(r,t)$ and $P(t)$ is treated as a parameter. The boundary conditions for the perturbations depend on the value of the azimuthal wavenumber n and are derived, for example, in Batchelor & Gill (1962). The following no-slip conditions for the functions u', v', w' and p' are used at the rigid boundary $r = 1$ for all n:

$$u'(1) = 0, \quad v'(1) = 0, \quad w'(1) = 0, \quad p'(1) = 0 \qquad \text{for all } n. \tag{38}$$

The conditions at $r = 0$ have the form

$$u'(0) = 0, \quad v'(0) = 0, \quad w'(0) \equiv \text{finite}, \quad p'(0) \equiv \text{finite} \qquad \text{if} \quad n = 0, \tag{39}$$

$$u'(0) + \mathrm{i}v'(0) = 0, \quad \left(2\frac{\mathrm{d}u'}{\mathrm{d}r} + \mathrm{i}\frac{\mathrm{d}v'}{\mathrm{d}r}\right)\Bigg|_{r=0} = 0, \quad w'(0) = 0, \quad p'(0) = 0 \qquad \text{if} \quad n = 1, \tag{40}$$

$$u'(0) = 0, \quad v'(0) = 0, \quad w'(0) = 0, \quad p'(0) = 0 \qquad \text{if} \quad n > 1. \tag{41}$$

Equations (34)–(37) together with boundary conditions (38), (39), (40) or (41) form an eigenvalue problem. The eigenvalues, $\gamma_m = \gamma_{rm} + \mathrm{i}\gamma_{im}$, $m = 1, 2, \ldots$, determine the stability of the base flow W. The flow is stable if $\gamma_{rm} > 0$ for all m and unstable if $\gamma_{rm} < 0$ for at least one value of m. The real part of γ is proportional to the growth rate of perturbations while the imaginary part of γ is proportional to the phase speed.

The system (34)–(37) and the boundary conditions (38)–(41) depend on many parameters, namely Re, t, α and n. For fixed values of t and n the set of numbers $Re = Re(\alpha)$ is determined as a function of α in the case when only one eigenvalue has zero real part, while the others have positive real parts. Then the critical Reynolds numbers are found by setting $Re^c = \min_\alpha Re(\alpha)$. This procedure is repeated for other sets of t and n. A collocation method based on Chebyshev polynomials is used to obtain the numerical solution to (34)–(41); details can be found in Khorrami, Malik & Ash (1989). A generalized eigenvalue problem of the form

$$(A - \gamma B)\psi = 0 \tag{42}$$

Case	$\tilde{t}_0$ (s)	$\tilde{t}_1$ (s)	$\tilde{t}_2$ (s)	$U_p\,(\mathrm{m\,s^{-1}})$	$\frac{0-U_p}{\tilde{t}_2-\tilde{t}_1}\,(\mathrm{m\,s^{-2}})$	$\tilde{t}_p$ (s)	δ_1/R
I	0.13	10.26	10.27	0.054	−5.4	19.2	0.85
II	0.42	3.68	4.04	0.16	−0.44	6.24	0.55
III	0.14	1.86	2.46	0.33	−0.55	2.76	0.39
IV	0.13	0.44	1.10	0.33	−0.5	1.80	0.18

TABLE 1. Parameters for the four experimental cases considered.

obtained by discretizing system (34)–(37) is solved by IMSL routine DGVLCG. The code was validated by reproducing the eigenvalues in tables VII–IX of Khorrami *et al.* (1989) for pipe Poiseuille flow. The results of linear stability calculations are used below to interpret the experimental data of DA. However, prior to re-interpreting the experiments of DA, it must be noted that the main motivation for adopting the *ad-hoc* approach and not the self-consistent approach of Cowley (1987) is to calculate the neutral stability curves. Near the neutral curve, the growth rate tends to zero and the reliability of the *ad-hoc* approach and the stability results derived from it, cannot, in general, be ascertained. Nevertheless, Cowley (1987, p. 263) noted 'Allmen and Eagles (1984) have shown recently that this heuristic approximation can sometimes be surprisingly good'. In this paper, the computed and the measured wavelength and the theoretically predicted and the observed type of instability are, generally, in reasonable agreement. Similar agreement between measured and computed stability results has also been reported in other papers (e.g. Gad-el-Hak *et al.* 1984; Krane & Gebhart 1993; and DA). However, in the absence of experimental data, the stability results obtained from the *ad-hoc* quasi-steady approach are, at best, suspect.

4. Results of linear stability calculations and discussion

Experimental and theoretical results obtained by DA are briefly described first. DA constructed a novel experimental approach for studying the transition to turbulence of unsteady velocity profiles with reverse flow in a pipe. The test rig consisted of a pipe–piston system. The flow of an incompressible fluid (water) was generated as follows: the velocity of the piston linearly increases from zero to some constant velocity U_p for $0 < \tilde{t} < \tilde{t}_0$, maintains a constant value U_p for $\tilde{t}_0 < \tilde{t} < \tilde{t}_1$, linearly decreases to zero for $\tilde{t}_1 < \tilde{t} < \tilde{t}_2$, and maintains a velocity of zero for $\tilde{t} > \tilde{t}_2$. The values of $\tilde{t}_0$, $\tilde{t}_1$ and $\tilde{t}_2$ for each of the four cases considered are given in table 1. This table also includes the experimentally observed time $\tilde{t}_p$ at which the instability sets in, the dimensionless boundary layer thickness δ_1/R at $\tilde{t} = \tilde{t}_1$ and the deceleration of the piston $(0 - U_p)/(\tilde{t}_2 - \tilde{t}_1)$.

DA reported that the instability observed in the experiments is helical (non-axisymmetric) when $\delta_1/R > 0.4$ but were unable to ascertain the type of instability when $\delta_1/R < 0.4$. With the view of providing insight into the experimentally observed instability, DA applied a linear stability analysis to the piston-generated unsteady base flow $W(r,t)$. The expression for $W(r,t)$ in the form of an infinite series containing Bessel functions was derived using a Laplace transform. The linear stability analysis of the base flow $W(r,t)$ performed by DA involved the planar geometry and quasi-steady assumptions. The use of the planar geometry assumption neglects the effects of curvature on the stability results such as the neutral stability curve. Intuitively, one

expects the curvature effects to be negligible and the planar geometry assumption to give reasonable estimates for the stability characteristics of the flow in the pipe for small δ_1/R values, where R is the pipe radius. However, as table 1 shows, the values of δ_1/R considered by DA in their experiment and analysis are not always small and varied from 0.18 to 0.85. The experiments showed that, in some cases, the non-axisymmetric modes are the least stable modes. Therefore, given that some of the experiments were conducted for large δ_1/R, where curvature effects may not be neglected, the planar geometry assumption is removed in this section and its validity is investigated by comparing the current stability results with those in DA. In addition, the stability of both axisymmetric and non-axisymmetric modes is investigated and the results used to re-interpret the experimental instabilities observed by DA. Both the present analysis and that of DA employs the quasi-steady assumption.

4.1. *Evaluation of the planar geometry assumption*

Calculations of the critical Reynolds numbers versus time for the four cases (i.e. Cases I–IV) are shown in figures 2–5 for different values of the azimuthal wavenumber n. Circles on the figures indicate the results obtained by DA with the planar geometry assumption. The Reynolds number in all these figures is defined as in DA, that is $Re_\delta = (U_{max} - U_{min})\delta/v$, where U_{max} and U_{min} are the maximum and minimum velocities of the base flow at a given instant and δ is the local boundary layer thickness.

Figures 2–5 show that the planar flow assumption correctly represents the qualitative behaviour of the stability curves. However, the relative error in calculating the critical Reynolds number depends on the case considered. The relative error is very small in Case IV since in this case the boundary layer thickness is the smallest so that the curvature of the pipe becomes negligible. On the other hand, the relative error in calculating the critical Reynolds number for Case I is as large as 60% since the boundary layer thickness is the largest among the four cases. In general, the smaller the boundary layer thickness, the better the quantitative agreement between the critical Reynolds numbers calculated for planar geometry assumption and for a pipe flow.

Note that the similarity between planar geometry stability results and circular geometry stability results for small δ/R values has been found by other researchers. For example, Davey & Nguyen (1971) performed a stability analysis of pipe flows subject to perturbations concentrated near the pipe wall and argued that the results are relevant to plane Couette flow. In addition, Ramaprian & Muller (1980) studied the transitional periodic boundary layer in a plane channel and found good agreement with the pipe flow results of Hino, Sawamoto & Takasu (1976) when $\delta/R \approx 0.25$. Nevertheless, Ramparian & Muller (1980) cautioned that the process of transition of a periodic oscillatory flow in a channel is, generally, significantly different from that in a pipe. Moreover, Akhavan *et al.* (1991) noted that the flow transition occurs at Reynolds number based on Stokes boundary layer thickness of about 500 for oscillatory flow pipes, channels and over flat plates (i.e. independent of the geometry). In fact, Akhavan *et al.* (1991) used the planar geometry for their numerical stability even though their experiments were carried in a pipe (circular geometry). This is feasible because their ratio of the boundary layer thickness to channel height was about 0.1. Furthermore, Sarpkaya (1993) stated that when δ/R is small, the results of oscillatory pipe flows are comparable with those over a flat plate. The present analysis, which compares the stability results in a pipe to those in a channel, is consistent with all these previous findings in that curvature effects are negligible for

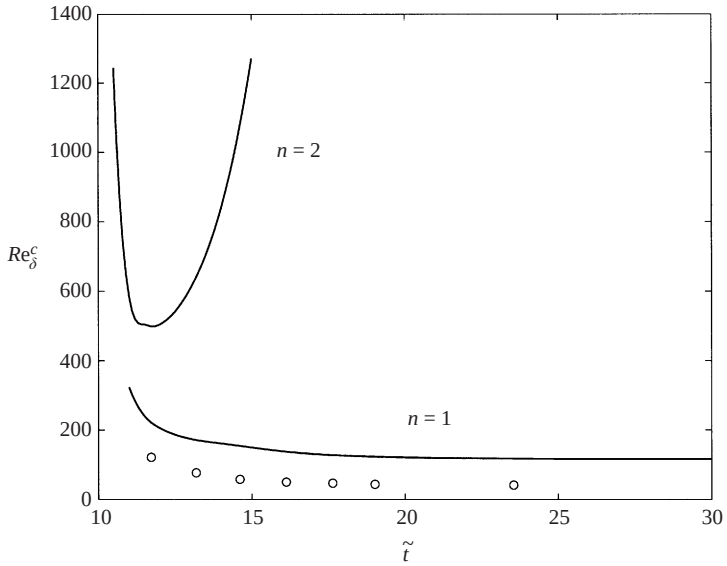

FIGURE 2. Critical Reynolds numbers Re_δ^c versus time for azimuthal modes with $n = 1$ and $n = 2$ (Case I). Circles represent the results of DA obtained with the planar geometry assumption.

small δ/R values. However, the authors caution against drawing similarities between unsteady flows in pipes, channels and over flat plates for large values of δ/R. That is, the three-dimensional stability analysis of unsteady pipe flows needs to be used when δ/R is large.

4.2. *Re-interpretation of the experimental data of DA*

Both the current stability analysis and the experiments of DA are conducted for flow in pipes. Therefore, the current stability analysis is used to understand and interpret the experimental instabilities observed by DA.

Figure 2 gives the results of the stability analysis for Case I (i.e. $\delta_1/R = 0.85$). This figure clearly shows that the most unstable mode is $n = 1$ (non-axisymmetric mode). No axisymmetric instability is found in the range of the Reynolds numbers and time shown in figure 2. Therefore, both the current analysis and the experiments of DA show that the helical mode is the least stable for Case I.

Figure 3 shows the results of the stability analysis for Case II (i.e. $\delta_1/R = 0.55$). The computational results show that the instability is also associated with a non-axisymmetric mode ($n = 1$). The graphs in figure 3 indicate that the mode with $n = 1$ is the least stable, at least for $\tilde{t} > 5$ s. For smaller values of time, the two graphs are very close to each other. The numerical values show that the curve for $n = 1$ lies below the curve for $n = 0$ for all values of time displayed in figure 3. However, given that the mathematical model involves a number of approximations, it is difficult to ascertain which of the two modes is the least stable in the range $\tilde{t} < 5$ s. DA found that the experimentally observed instability waves formed at $\tilde{t} = 6.24$ s and that there is phase difference of approximately 180° between vortices at the top and bottom of the pipe (i.e. helical instability). Clearly, $\tilde{t} = 6.24$ s belongs to the range where the non-axisymmetric mode $n = 1$ is the least stable and helps explain why a helical instability appeared in Case II of the experiments of DA.

Figures 4 and 5 show the results of the stability analysis for Case III (i.e. $\delta_1/R =$

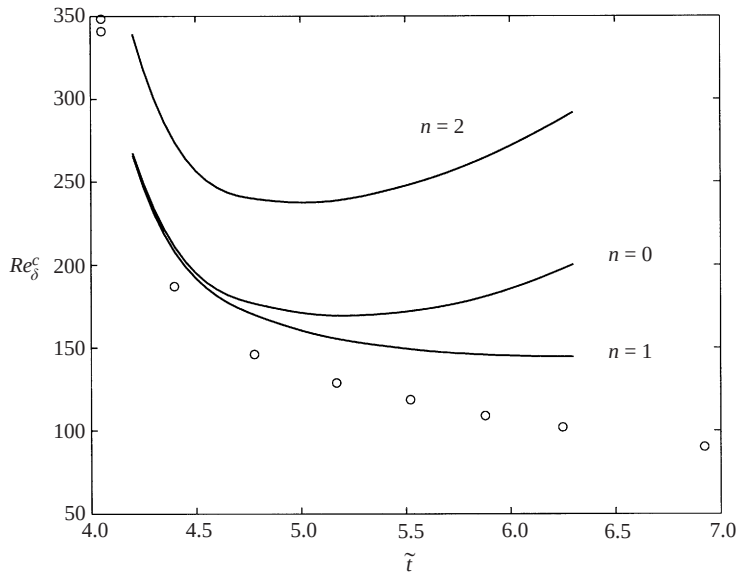

FIGURE 3. As figure 2 but for Case II and $n = 0$, $n = 1$ and $n = 2$.

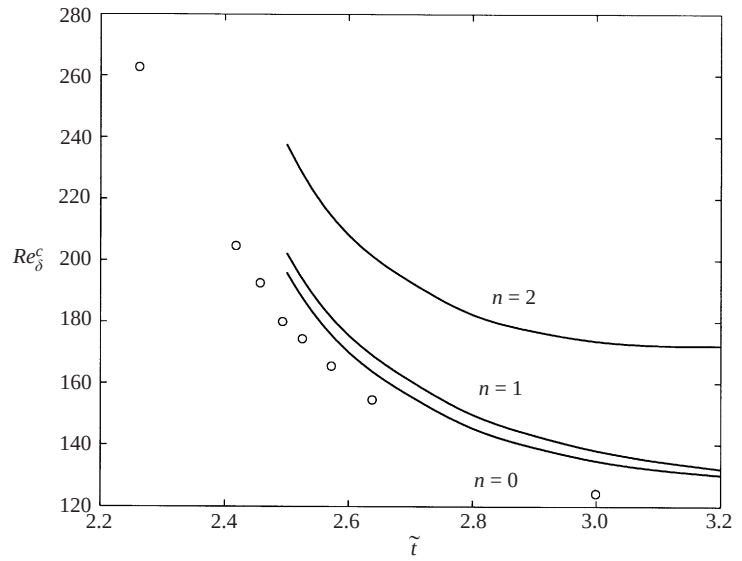

FIGURE 4. As figure 2 but for Case III and $n = 0$, $n = 1$ and $n = 2$.

0.39) and Case IV (i.e. $\delta_1/R = 0.18$), respectively. These figures indicate that the neutral stability curve of the axisymmetric mode $n = 0$ and the neutral stability curve for the helical mode $n = 1$ are very close to one another. However, the calculations show that the most unstable mode in Case III and Case IV is the axisymmetric mode. As has been pointed out by DA (p. 261): 'In many of the experiments, especially when $\delta_1/R < 0.4$, the waves/vortices do not form simultaneously on the top and bottom walls... In these cases it is also not possible to ascertain whether the phase difference between top and bottom wall vortices is 180 degrees, i.e. whether the mode is helical'.

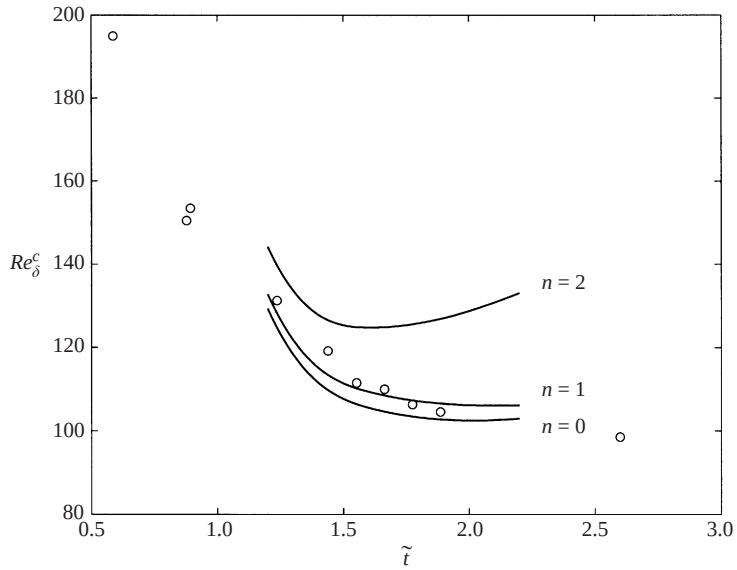

FIGURE 5. As figure 2 but for Case IV and $n = 0$, $n = 1$ and $n = 2$.

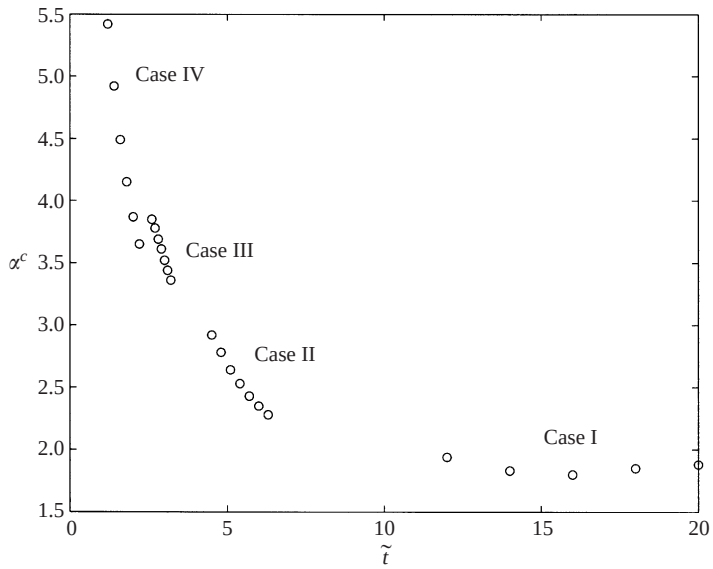

FIGURE 6. Critical wavenumbers α^c versus time for all four cases.

Hence, the results of calculations are in qualitative agreement (in terms of the pattern of the most unstable mode) with the experiments of DA for all four cases.

Figure 6 plots the critical axial wavenumbers, α^c, scaled with the radius of the pipe, R, versus time for all four cases. It is seen from the figure that, for example, the critical wavenumbers for Case III are larger than those for Case I and Case II. In other words, the spacing between the vortices in Case III has decreased in comparison with Case I and Case II – a result that is consistent with the experimental observations of DA.

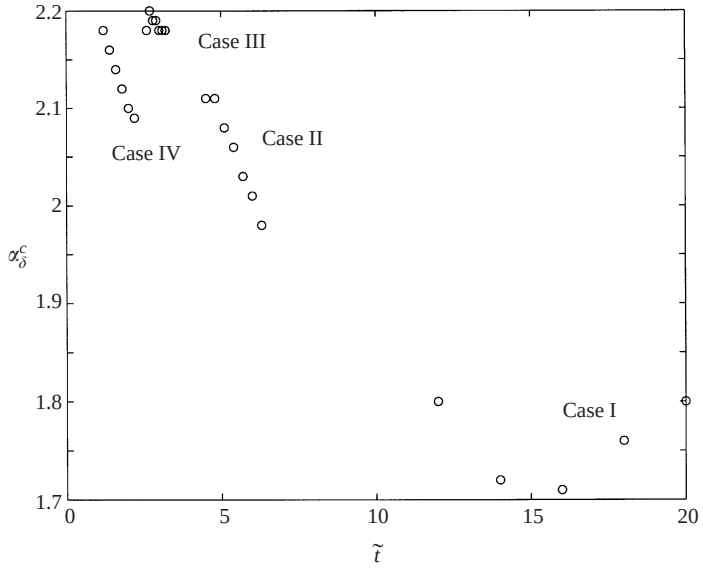

FIGURE 7. Critical wavenumbers α_δ^c versus time for all four cases.

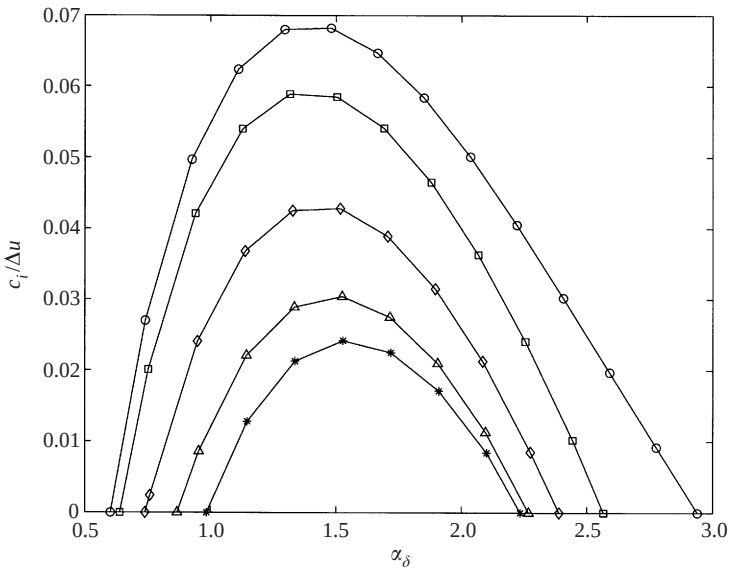

FIGURE 8. Growth rates of perturbations normalized by $\Delta u = U_{max} - U_{min}$ versus α_δ at different times: curve with circles for $\tilde{t} = 12$ s; curve with rectangles for $\tilde{t} = 14$ s; curve with diamonds for $\tilde{t} = 16$ s; curve with triangles for $\tilde{t} = 18$ s; curve with stars for $\tilde{t} = 19.2$ s (Case I).

The critical axial wavenumbers, α_δ^c (scaled with δ, the thickness of the local boundary layer, which is defined as the distance from the wall at which the velocity reaches 99% of the velocity U_{max}), are re-plotted in figure 7. It is seen from the figure that for each particular case α_δ^c does not change much during the development of instability. A qualitatively similar result is obtained with the planar flow assumption in DA.

Case	$(\lambda/\delta_*)_{exp}$	$(\lambda^c/\delta_*)_{DA}$	$(\lambda_{max}/\delta_*)_{DA}$	λ^c/δ_*	λ_{max}/δ_*
I	3.2	3.3	4.0	3.6	3.7
II	2.7	3.4	4.2	3.0	2.8
III	3.1	3.4	5.0	2.8	2.7
IV	3.0	2.8	3.3	2.9	2.6

TABLE 2. Comparison of scaled wavelengths.

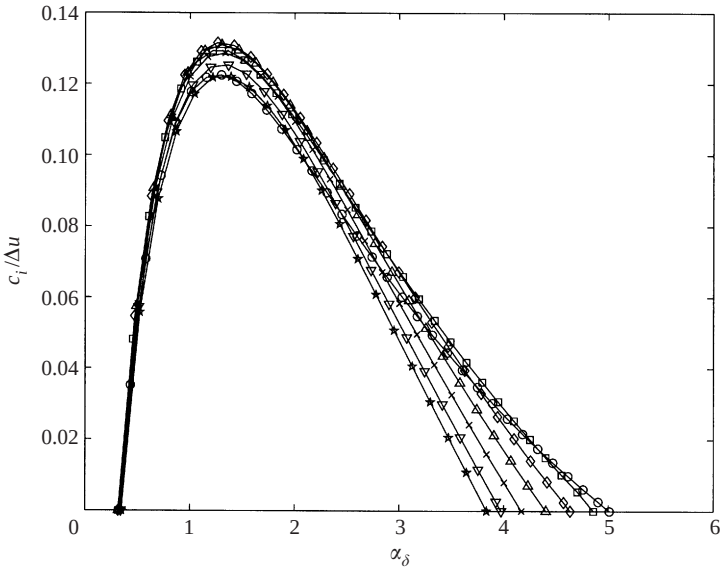

FIGURE 9. Growth rates of perturbations normalized by $\Delta u = U_{max} - U_{min}$ versus α_δ at different times: curve with circles for $\tilde{t} = 4.8$ s; curve with rectangles for $\tilde{t} = 5.1$ s; curve with diamonds for $\tilde{t} = 5.4$ s; curve with triangles for $\tilde{t} = 5.7$ s; curve with crosses for $\tilde{t} = 6.0$ s; curve with solid triangles for $\tilde{t} = 6.2$ s; and curve with stars for $\tilde{t} = 6.24$ s (Case II).

The experimentally obtained wavelength, λ, scaled with δ_* is compared with $(\lambda^c/\delta_*)_{DA}$, $(\lambda_{max}/\delta_*)_{DA}$, λ^c/δ_* and λ_{max}/δ_*. (Here δ_* is the average boundary layer thickness taken over the time $\tilde{t}_1$ to $\tilde{t}_p$. This time interval $\tilde{t}$ is divided into several subintervals of constant width and the boundary layer thickness δ is evaluated at each of the endpoints of the subintervals; δ_* is just the average of δ values.) The results of comparison are shown in table 2. The subscript DA in table 2 refers to the results of DA, obtained with the planar flow assumption, λ^c corresponds to the critical Reynolds number Re_δ^c and λ_{max} corresponds to maximum growth rate. It is seen from table 2 that experimentally observed wavelengths are close to the calculated values of λ. Both the present analysis, which incorporates the effects of pipe curvature, and the analysis of DA, which ignores the effect of pipe curvature, produce wavelengths that are in reasonable agreement with the experimental wavelength of perturbations. As a result, it appears that the wavelength of the instability is not sensitive to pipe curvature.

Growth rates of disturbances normalized by $\Delta u = U_{max} - U_{min}$ (where $c_i = -\gamma_r/\alpha_\delta$) for all four cases versus α_δ are plotted in figures 8–11 for different values of the time. It is shown in DA under the planar flow assumption that the normalized growth rates collapse onto a single curve when scaled with instantaneous Δu and δ. The

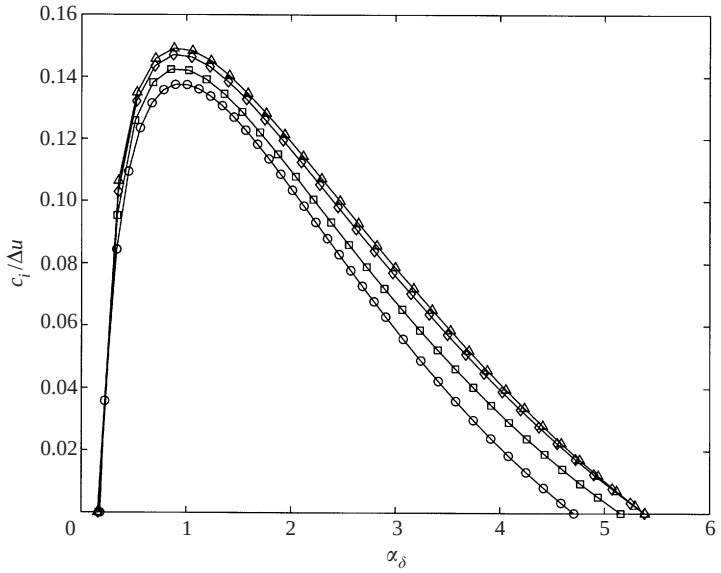

FIGURE 10. Growth rates of perturbations normalized by $\Delta u = U_{max} - U_{min}$ versus α_δ at different times: curve with circles for $\tilde{t} = 2.5\,\mathrm{s}$; curve with rectangles for $\tilde{t} = 2.6\,\mathrm{s}$; curve with diamonds for $\tilde{t} = 2.7\,\mathrm{s}$; and curve with triangles for $\tilde{t} = 2.76\,\mathrm{s}$ (Case III).

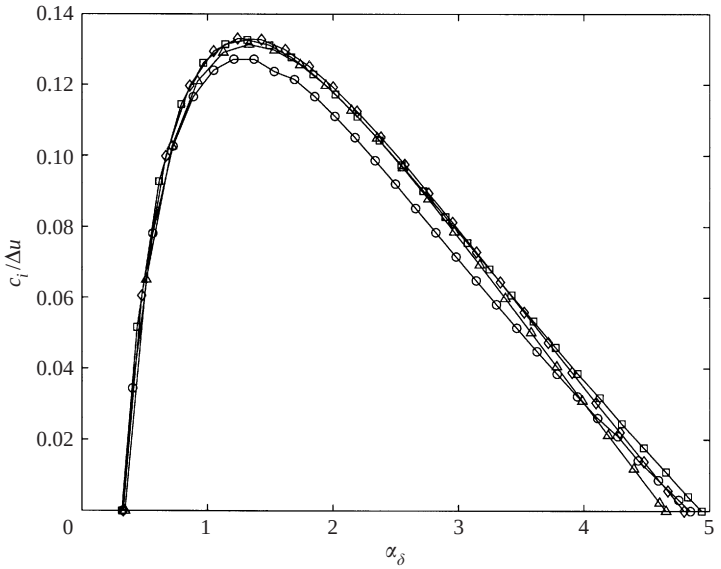

FIGURE 11. Growth rates of perturbations normalized by $\Delta u = U_{max} - U_{min}$ versus α_δ at different times: curve with circles for $\tilde{t} = 1.2\,\mathrm{s}$; curve with rectangles for $\tilde{t} = 1.4\,\mathrm{s}$; curve with diamonds for $\tilde{t} = 1.6\,\mathrm{s}$; and curve with triangles for $\tilde{t} = 1.8\,\mathrm{s}$ (Case IV).

graphs in figures 9–11 show that this conclusion is true when the boundary layer thickness is not too large. Comparing figure 12(*b*) in DA and figures 8–11, one can see that the normalized maximum growth rates are overestimated by the planar flow assumption. The error in normalized maximum growth rate is small for Case III and Case IV. However, the calculated normalized maximum growth rates for Case I (figure 8) are approximately two times larger than those calculated with the planar

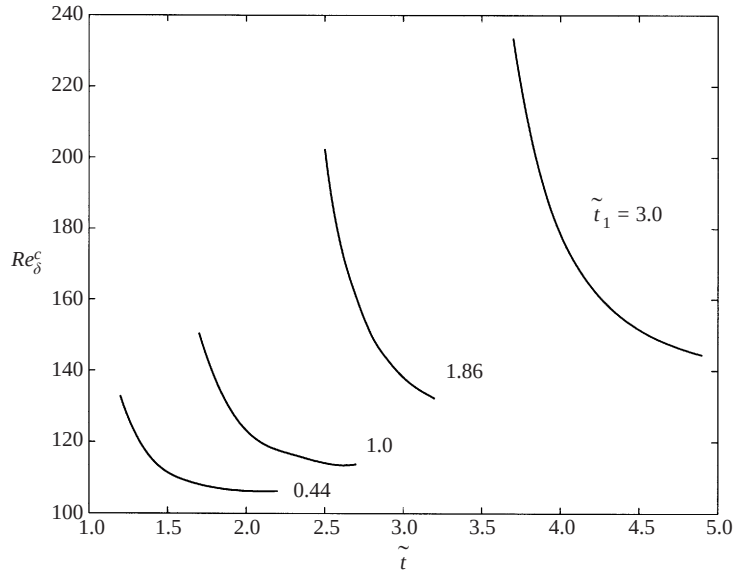

FIGURE 12. Critical Reynolds numbers Re_δ^c versus time for azimuthal mode with $n = 1$ for different values of $\tilde{t}_1$.

flow assumption. Recall that the error in calculating the critical Reynolds numbers with the planar flow assumption is also large for Case I. This means that in order to obtain reliable stability characteristics for rapidly decelerating flows which were developed prior to deceleration, the full three-dimensional stability equations for pipe flow should be used.

4.3. *Effects of the time of flow development on the stability characteristics*

Figure 12 shows the critical Reynolds numbers Re_δ^c calculated for fixed values of $\tilde{t}_0 = 0.13\,\mathrm{s}$, $\tilde{t}_2 - \tilde{t}_1 = 0.6\,\mathrm{s}$ and different values of $\tilde{t}_1$. Hence, the stability curves in figure 12 correspond to constant acceleration and deceleration rates and different times of development of the flow ($\tilde{t}_1$). It is seen from the figure that the critical Reynolds number Re_δ^c increases as $\tilde{t}_1$ grows. Hence, the increase in time of the development of the flow has a stabilizing influence on the base flow. The maximum growth rate $\gamma^{max} = \max_\alpha(-\gamma_r)$ for $n = 1$ and $Re = UR/\nu = 1000$ is shown in figure 13 for four values of $\tilde{t}_1$. It increases immediately after the deceleration phase (small values of $\tilde{t} - \tilde{t}_2$), reaches a maximum and then decreases. The position and the value of the maximum depends on $\tilde{t}_1$. For relatively small values of $\tilde{t}_1$ the maximum increases as $\tilde{t}_1$ increases (see the curves for $\tilde{t}_1 = 1.0\,\mathrm{s}$, $1.86\,\mathrm{s}$ and $3.0\,\mathrm{s}$). For larger values of $\tilde{t}_1$ the growth rates become more uniform over the whole period of the development of the instability (see the curve for $\tilde{t}_1 = 3\,\mathrm{s}$).

4.4. *Effects of deceleration rate on the stability characteristics*

Experiments in DA were performed for different values of the parameters of the problem. However, a systematic study of the effect of the deceleration rate on the stability boundary was not performed because there was not much control over the time $\tilde{t}_2 - \tilde{t}_1$. Some results on the influence of the deceleration rate on the stability characteristics of the flow are presented below.

Consider a fully developed Poiseuille flow in a pipe. Suppose that at $\tilde{t} = 0$ the flow

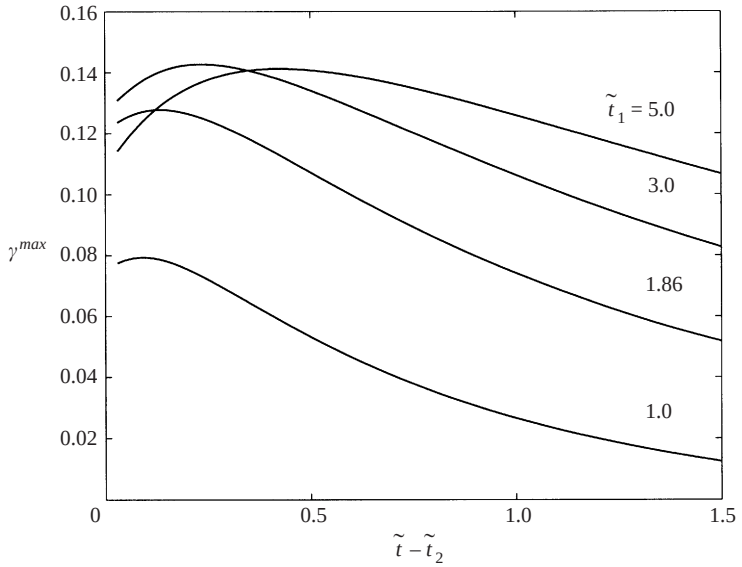

FIGURE 13. Maximum growth rates $\gamma^{max} = \max_\alpha(-\gamma_r)$ for $n = 1$ and $Re = 1000$ versus $\tilde{t} - \tilde{t}_2$ for different values of $\tilde{t}_1$.

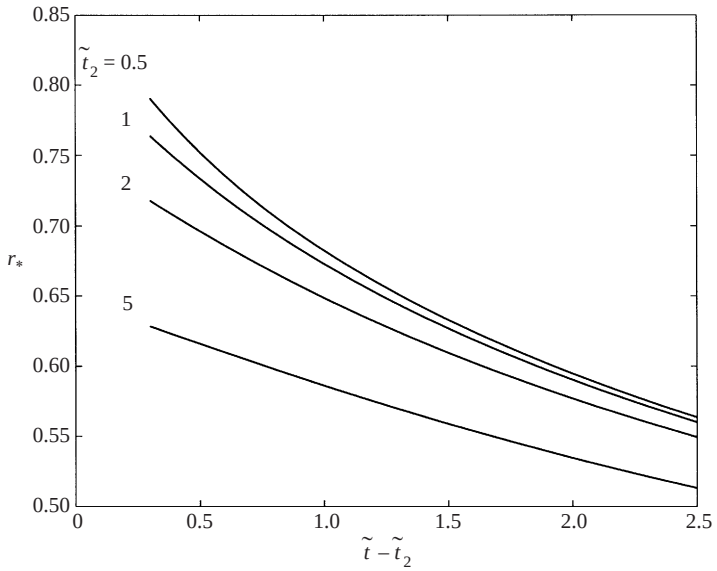

FIGURE 14. Location of inflection point r_* versus $\tilde{t} - \tilde{t}_2$ for different values of $\tilde{t}_2$.

is linearly decelerated to zero over the time interval $[0, \tilde{t}_2]$. Base velocity profiles for $\tilde{t} > \tilde{t}_2$ have inflection points. In fact, the critical Reynolds number depends on the position of the inflection point. The location of inflection point r_* versus $\tilde{t} - \tilde{t}_2$ is shown in figure 14 for different values of $\tilde{t}_2$. It is seen from the figure that as time increases, the inflection point moves towards the centre of the pipe. However, the rate of change of the location of the inflection point depends on the value of $\tilde{t}_2$: the more violent the transient, the larger the rate of change of the inflection point with respect to time. The farther away the inflection point is from the wall, the more unstable the

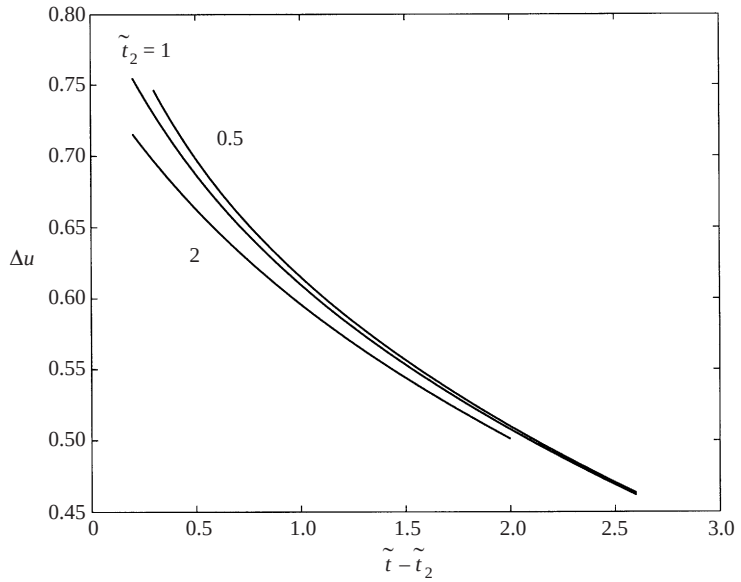

FIGURE 15. The variation of $U_{max} - U_{min}$ versus $\tilde{t} - \tilde{t}_2$ for different values of $\tilde{t}_2$.

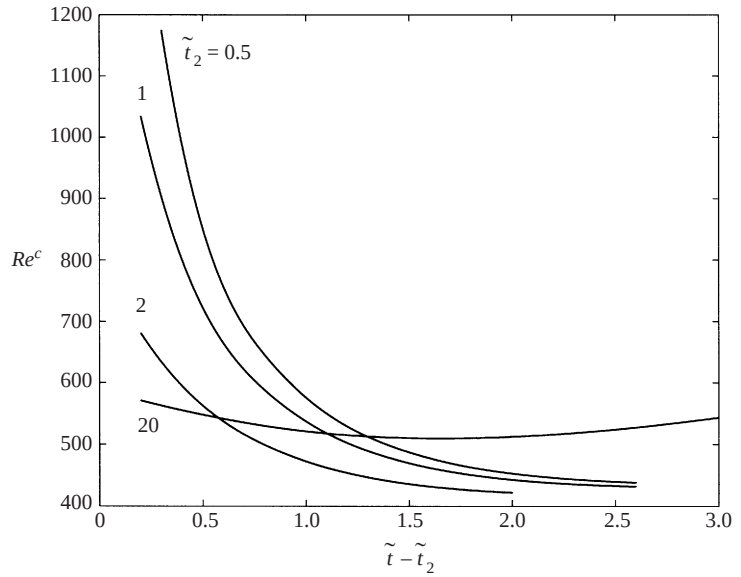

FIGURE 16. Critical Reynolds numbers Re^c versus time for azimuthal mode with $n = 1$ for different values of $\tilde{t}_2$.

flow. On the other hand, as time increases, the difference between the maximum and minimum velocity decreases. As a result, the Reynolds number based on $U_{max} - U_{min}$ decreases and the flow becomes more stable. The variation of $U_{max} - U_{min}$ versus time for three values of $\tilde{t}_2$ is shown in figure 15. Again, the rate of change of the difference $U_{max} - U_{min}$ versus time is larger for smaller values of $\tilde{t}_2$.

The development of instability depends on the competing influence of the two factors mentioned above, namely the movement of the inflection point towards the centre of the pipe and the reduction of the difference $U_{max} - U_{min}$ as time increases. The

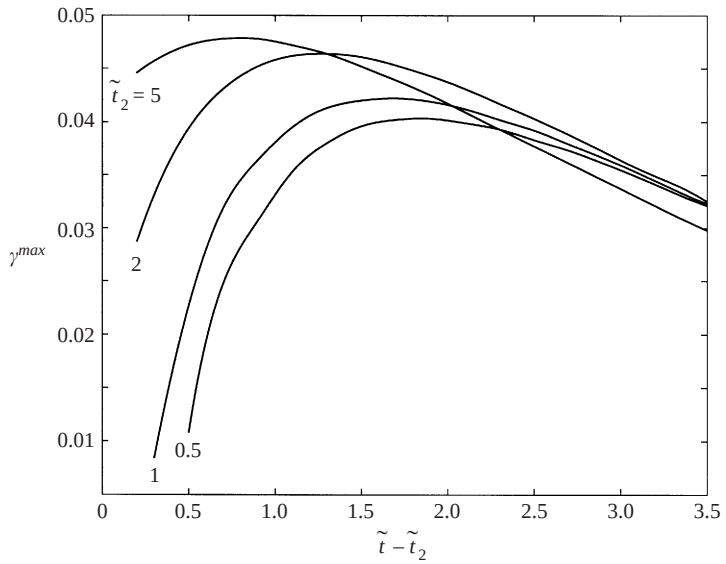

FIGURE 17. Maximum growth rates $\gamma^{max} = \max_\alpha(-\gamma_r)$ for $n = 1$ and $Re = 1000$ versus $\tilde{t} - \tilde{t}_2$ for different values of $\tilde{t}_2$.

critical Reynolds numbers Re^c (based on the maximum velocity of the undisturbed flow U and the radius of the pipe R) versus $\tilde{t} - \tilde{t}_2$ are shown in figure 16 for different values of the deceleration time $\tilde{t}_2$. It is seen from the figure that as the deceleration time increases (see the curves for $\tilde{t}_2 = 0.5$ s, 1 s and 2 s), the critical Reynolds numbers decrease. However, for larger values of $\tilde{t} - \tilde{t}_2$ the difference between the values of Re^c becomes smaller. On the other hand, if the deceleration time is large (see the curve for $\tilde{t}_2 = 20$ s) then the minimal critical Reynolds number is larger than for the previous three cases. Moreover, the rate of change of the critical Re versus time also depends on the value of $\tilde{t}_2$: the smaller the deceleration time is, the larger the decrease of Re^c versus time.

Maximum growth rates $\gamma^{max} = \max_\alpha(-\gamma_r)$ for $n = 1$ and $Re = 1000$ versus $\tilde{t} - \tilde{t}_2$ are shown in figure 17 for different values of the deceleration time $\tilde{t}_2$. It is seen from the figure that the growth rates differ considerably during the initial time of the development of the instability (small values of $\tilde{t} - \tilde{t}_2$). However, the difference between the growth rates becomes smaller as $\tilde{t} - \tilde{t}_2$ increases.

4.5. *Verification of the quasi–steady assumption*

As has already been pointed out, the quasi-steady assumption is justified if the growth rates of perturbations are considerably larger than the rate of change of the base flow with respect to time. In order to compare these two values one needs to compare $\partial \ln W_*/\partial t_*$ and $\gamma_* = \partial \ln w_*/\partial t_*$, where the asterisks represent dimensional variables. Since our calculations are done in dimensionless form, the corresponding dimensionless quantities should be compared. Using diffusion time scale R^2/ν and the representation $\gamma_* = \alpha_* c_* = \alpha c U_{max}/R$, it can be seen that the comparison should be made between $\partial \ln W/\partial t$ and γRe. Note that this choice of scaling for γ_* is justified because only the product γRe appears in the stability equations. Therefore it is natural to introduce the following ratio:

$$\eta = \left| \frac{1}{W} \frac{\partial W}{\partial t} / [\gamma^{max} Re] \right|,$$

Time (s)	$\eta\|_{r=0}$	$\eta\|_{r=0.2}$	$\eta\|_{r=0.5}$	$\eta\|_{r=0.6}$	$\eta\|_{r=0.8}$	$\eta\|_{r=0.9}$
11	0.0022	0.0025	0.0057	0.0008	0.0106	0.0136
12	0.0016	0.0019	0.0055	0.0039	0.0065	0.0228
13	0.0019	0.0023	0.0070	0.0047	0.0063	0.1344
14	0.0026	0.0031	0.0091	0.0069	0.0068	0.0126
15	0.0037	0.0044	0.0117	0.0072	0.0081	0.0041
16	0.0054	0.0062	0.0151	0.0091	0.0100	0.0002
17	0.0079	0.0088	0.0194	0.0119	0.0127	0.0039
18	0.0113	0.0124	0.0249	0.0155	0.0164	0.0081
19.2	0.0174	0.0185	0.0336	0.0219	0.0228	0.0146
4.5	0.00056	0.00057	0.00100	0.00182	0.00048	0.00217
5.0	0.00045	0.00048	0.00111	0.00242	0.00062	0.00202
5.5	0.00043	0.00048	0.00138	0.00344	0.00107	0.00203
6.0	0.00044	0.00053	0.00180	0.00498	0.00138	0.00213
6.24	0.00046	0.00057	0.00200	0.00606	0.00150	0.00219
2.6	0.00043	0.00043	0.00051	0.00075	0.00139	0.00092
2.7	0.00044	0.00044	0.00052	0.00078	0.00143	0.00095
2.76	0.00045	0.00045	0.00054	0.00080	0.00146	0.00097
1.3	0.00084	0.00084	0.00085	0.00098	0.00849	0.00158
1.5	0.00108	0.00108	0.00110	0.00127	0.01096	0.00203
1.7	0.00138	0.00138	0.00139	0.00161	0.01390	0.00258
1.8	0.00154	0.00154	0.00156	0.00180	0.01554	0.00288

TABLE 3. Calculations of the value of η for different values of r and $\tilde{t}$. (*a*) Case I, $Re = 684$; (*b*) Case II, $Re = 2037$; (*c*) Case III, $Re = 4251$; (*d*) Case IV, $Re = 4251$.

where $\gamma^{max} = \max_{\alpha}(-\gamma_r)$ is the maximal growth rate at a given instant. The value γ^{max} is calculated for the spiral mode ($n = 1$) for Case I and Case II and for the axisymmetric mode ($n = 0$) for Case III and Case IV. If η is considerably smaller than 1, then the quasi-steady approach is justified. Clearly, η depends on r and $\tilde{t}$. Calculations of the values of η for different values of r and $\tilde{t}$ are shown in table 3. Note that for each $\tilde{t} > \tilde{t}_2$ there is a point in the interval $0 < r < 1$ where $W = 0$, so that η is not defined at that point. However, we believe that the validity of the quasi-steady approach depends on the global behaviour of η and a singular point will not be important. All the values of time in table 3 are given in seconds and the last row in each case corresponds to the time where the instability was observed first in all four cases of the experiments by DA. The Reynolds number in table 3 is defined as follows: $Re = U_p R/\nu$. It is seen from table 3 that the value of η is considerably smaller than 1 (i.e. $\eta \ll 1$) for all four cases considered. This means that the quasi-steady stability analysis gives reasonable results for the time-dependent pipe flows studied by DA and in this paper.

5. Weakly nonlinear analysis

5.1. *Derivation of the Ginzburg–Landau equation*

The results of the linear stability calculations indicate that in some cases (see, for example, Case III and Case IV in DA) the most unstable mode is the axisymmetric mode with $n = 0$. It is shown in this section by means of weakly nonlinear theory that in such a case the amplitude evolution equation near the threshold is the complex Ginzburg–Landau equation.

Introducing the stream function $\psi(r, z, t)$ by the relations

$$u = -\frac{\psi_z}{r}, \quad w = \frac{\psi_r}{r}, \tag{43}$$

the system of Navier–Stokes equations (under the assumption that $v = 0$) reduces to a single equation for the stream function ψ.

Consider now a perturbed solution to the Navier–Stokes equation of the form

$$\psi = \psi_0 + \varepsilon\psi_1 + \varepsilon^2\psi_2 + \varepsilon^3\psi_3 + \cdots, \tag{44}$$

where ε is a small parameter. Note that we use the same symbol ε to denote a small parameter as in the section where the asymptotic solution is derived. However, these two parameters are not the same and ε is chosen here simply because this notation is a standard one. Let us assume first that only two terms on the right-hand side of (44) are taken into account. Substituting (44) into the Navier–Stokes equation, linearizing in the neighbourhood of the base flow, collecting the terms of order ε and assuming that the perturbation $\psi_1(r, z, t)$ has the form

$$\psi_1(x, y, t) = \varphi_1(r)\exp[\mathrm{i}\alpha(z - ct)] + \text{c.c.} \tag{45}$$

(c.c. means 'complex conjugate') we obtain

$$\mathrm{L}_1\varphi_1 = 0, \tag{46}$$

where the operator L_1 is given by

$$\mathrm{L}_1\varphi \equiv \varphi'''' - \frac{2}{r}\varphi''' + \varphi''\left(\frac{3}{r^2} - 2\alpha^2 - \mathrm{i}kReW\right) + \varphi'\left(-\frac{3}{r^3} + \frac{2\alpha^2}{r} + \frac{\mathrm{i}\alpha WRe}{r}\right)$$
$$+ \varphi\left(\alpha^4 + \mathrm{i}\alpha ReW'' - \frac{\mathrm{i}\alpha ReW'}{r} + \mathrm{i}\alpha^3 WRe\right) + \mathrm{i}\alpha cRe\left(\varphi'' - \frac{\varphi'}{r} - \alpha^2\varphi\right), \tag{47}$$

with $Re = UR/v$.

The function φ_1 satisfies the following boundary conditions:

$$\varphi_1(0) = 0, \quad \varphi_1(1) = 0, \quad \varphi_{1r}(0) = 0, \quad \varphi_{1r}(1) = 0. \tag{48}$$

Linear stability problem (34)–(39) can be reduced to the form (46)–(48) for the case of axisymmetric perturbations with $n = 0$. Thus, the critical values of α and Re can be calculated for any given transient scenario. In particular, for Case III at $\tilde{t} = 2.8$ s, $\alpha_c = 3.6949$, $Re_c = 499.3265$ and $c_c = 0.03256$. The imaginary part of c for the case $\alpha = \alpha_c$ and $Re = Re_c$ is very small: $c_i = 0.000000007$. If $\alpha = \alpha_c$ and $Re = Re_c$ then the function $\varphi_1(r)$ is an eigenfunction of the linear stability problem. In order to study the nonlinear evolution of the most unstable perturbation when the value of Re is slightly above the critical value Re_c, the method of multiple scales is used (see Kevorkian & Cole 1996; Drazin & Reid 1981, and references therein).

In particular, we assume that

$$Re = Re_c(1 + \varepsilon^2). \tag{49}$$

Following the classical papers by Stuart (1960) and Stewartson & Stuart (1971) we introduce the 'slow' time τ and stretched longitudinal coordinate ξ which moves with a group velocity c_g:

$$\tau = \varepsilon^2 t, \quad \xi = \varepsilon(z - c_g t).$$

In this case the differential operators $\partial/\partial t$ and $\partial/\partial z$ are replaced by

$$\frac{\partial}{\partial t} \to \frac{\partial}{\partial t} - \varepsilon c_g \frac{\partial}{\partial \xi} + \varepsilon^2 \frac{\partial}{\partial \tau} \tag{50}$$

and

$$\frac{\partial}{\partial z} \to \frac{\partial}{\partial z} + \varepsilon \frac{\partial}{\partial \xi}, \tag{51}$$

respectively. The function ψ_1 in (44) is sought in the form

$$\psi_1 = A(\xi, \tau)\varphi_1(r) \exp[\mathrm{i}\alpha_c(z - c_c t)] + \text{c.c.}, \tag{52}$$

where $\varphi_1(r)$ is an eigenfunction of the linear stability problem, c_c is the wave speed at $\alpha = \alpha_c$, $Re = Re_c$ and A is a slowly varying amplitude.

In order to find the equation which describes the evolution of A one needs to consider higher terms of the perturbation expansion (44). Substituting (44), (49)–(51) into the Navier–Stokes equation and collecting the terms of order ε^2 gives

$$\begin{aligned}
\mathrm{L}_2\psi_2 = {} & c_g\left(\psi_{1rr\xi} - \frac{\psi_{1r\xi}}{r} + \psi_{1zz\xi}\right) - 2\psi_{1z\xi t} + \psi_{1\xi}\left(W'' - \frac{W'}{r}\right) + W\frac{\psi_{1r\xi}}{r} \\
& - W\psi_{1rr\xi} - 3W\psi_{1zz\xi} + \psi_{1z}\left(\frac{\psi_{1rrr}}{r} - \frac{3}{r^2}\psi_{1rr} + \frac{3}{r^3}\psi_{1r} + \frac{\psi_{1rzz}}{r} - 2\frac{\psi_{1zz}}{r^2}\right) \\
& + \psi_{1r}\left(\frac{\psi_{1rz}}{r^2} - \frac{\psi_{1rrz}}{r} - \frac{\psi_{1zzz}}{r}\right) \\
& + \frac{1}{Re_c}\left(4\psi_{1zzz\xi} + 4\psi_{1rrz\xi} - \frac{4}{r}\psi_{1rz\xi} - rW''' - W'' + \frac{W'}{r}\right),
\end{aligned} \tag{53}$$

where the operator L_2 is defined as follows:

$$\begin{aligned}
\mathrm{L}_2\varphi \equiv {} & \varphi_{rrt} - \frac{\varphi_{rt}}{r} + \varphi_{zzt} - \varphi_z\left(\frac{\psi_{0rrr}}{r} - 3\frac{\psi_{0rr}}{r^2} + 3\frac{\psi_{0r}}{r^3}\right) \\
& - \varphi_{rz}\frac{\psi_{0r}}{r^2} + \frac{\psi_{0r}}{r}(\varphi_{rrz} + \varphi_{zzz}) - \frac{1}{Re_c}\mathrm{L}\varphi.
\end{aligned} \tag{54}$$

Finally, collecting the terms of order ε^3 we obtain

$$\begin{aligned}
\mathrm{L}_2\psi_3 = {} & c_g\left(\psi_{2rr\xi} - \frac{\psi_{2r\xi}}{r} + \psi_{2zz\xi} + 2\psi_{1z\xi\xi}\right) - \psi_{1rr\tau} + \frac{\psi_{1r\tau}}{r} - \psi_{1zz\tau} - \psi_{1\xi\xi t} - 2\psi_{2z\xi t} \\
& + \psi_{2\xi}\left(W'' - \frac{W'}{r}\right) + \psi_{2r\xi}\frac{W}{r} + \frac{\psi_{2rz}}{r^2}\psi_{1r} - W(\psi_{2rr\xi} + 3\psi_{2zz\xi} + 3\psi_{1zz\xi}) \\
& + \psi_{2z}\mathrm{L}_3\psi_1 + \psi_{1z}\left(\mathrm{L}_3\psi_2 + 2\frac{\psi_{1rz\xi}}{r} - 4\frac{\psi_{1z\xi}}{r^2}\right) \\
& + \psi_{1\xi}\mathrm{L}_3\psi_1 + \psi_{2r}\left(\frac{\psi_{1rz}}{r^2} - \frac{\psi_{1rrz}}{r} - \frac{\psi_{1zzz}}{r}\right) \\
& + \psi_{1r}\left(\frac{\psi_{1r\xi}}{r^2} - \frac{\psi_{1rr\xi}}{r} - 3\frac{\psi_{1zz\xi}}{r} - \frac{\psi_{2rrz}}{r} - \frac{\psi_{2zzz}}{r}\right) \\
& - \frac{1}{Re_c}\left(\mathrm{L}\psi_1 - 6\psi_{1zz\xi\xi} - 2\psi_{1rr\xi\xi} + \frac{2}{r}\psi_{1r\xi\xi} - 4\psi_{2zzz\xi} - 4\psi_{2rrz\xi} + \frac{4}{r}\psi_{2rz\xi}\right),
\end{aligned} \tag{55}$$

where the operators L_3 and L are given by

$$\mathrm{L}_3\varphi \equiv \frac{\varphi_{rrr}}{r} - \frac{3}{r^2}\varphi_{rr} + \frac{3}{r^3}\varphi_r + \frac{\varphi_{rzz}}{r} - \frac{2\varphi_{zz}}{r^2}.$$

$$\mathrm{L}\varphi \equiv \varphi_{rrrr} + \varphi_{zzzz} + 2\varphi_{rrzz} - \frac{2}{r}\varphi_{rrr} + \frac{3}{r^2}\varphi_{rr} - \frac{3}{r^3}\varphi_r - \frac{2}{r}\varphi_{rzz}.$$

The form of the right-hand side of (53) and the form of the function ψ_1 (see (52)) suggests that the function ψ_2 should be sought in the following form:

$$\psi_2 = A^2\varphi_2^{(0)}(r)\exp[2\mathrm{i}\alpha_c(x-c_ct)] + AA^*\varphi_2^{(1)}(r) + A_\xi\varphi_2^{(2)}(r)\exp[\mathrm{i}\alpha_c(x-c_ct)] + \text{c.c.}, \quad (56)$$

where A^* denotes the complex conjugate of A.

Substituting (52) for ψ_1 and (56) for ψ_2 into (53) and collecting terms proportional to $A^2\exp[2\mathrm{i}\alpha_c(x-ct)]$ gives

$$\begin{aligned}
&2\mathrm{i}\alpha_c(W-c_c)\left(\varphi_{2rr}^{(0)} - \frac{\varphi_{2r}^{(0)}}{r} - 4\alpha_c^2\varphi_2^{(0)}\right) + 2\mathrm{i}\alpha_c\varphi_2^{(0)}\left(-W'' + \frac{W'}{r}\right)\\
&\quad + \frac{1}{Re_c}\left(-\varphi_{2rrrr}^{(0)} - 16\alpha_c^4\varphi_2^{(0)} + 8\alpha_c^2\varphi_{2rr}^{(0)} + \frac{2}{r}\varphi_{2rrr}^{(0)} - \frac{3}{r^2}\varphi_{2rr}^{(0)} + \frac{3}{r^3}\varphi_{2r}^{(0)} - \frac{8\alpha_c^2}{r}\varphi_{2r}^{(0)}\right)\\
&= \mathrm{i}\alpha_c\varphi_1\left(\frac{\varphi_{1rrr}}{r} - \frac{3}{r^2}\varphi_{1rr} + \frac{3}{r^3}\varphi_{1r} - \frac{\alpha_c^2}{r}\varphi_{1r} + 2\frac{\alpha_c^2}{r^2}\varphi_1\right)\\
&\quad + \mathrm{i}\alpha_c\varphi_{1r}\left(\frac{\varphi_{1r}}{r^2} - \frac{\varphi_{1rr}}{r} + \frac{\alpha_c^2}{r}\varphi_1\right) \qquad (57)
\end{aligned}$$

with the boundary conditions

$$\varphi_2^{(0)}(0) = 0, \quad \varphi_2^{(0)}(1) = 0, \quad \varphi_{2r}^{(0)}(0) = 0, \quad \varphi_{2r}^{(0)}(1) = 0. \quad (58)$$

Similarly, collecting the terms that are proportional to AA^* yields

$$\begin{aligned}
&\frac{1}{Re_c}\left(-\varphi_{2rrrr}^{(1)} + \frac{2}{r}\varphi_{2rrr}^{(1)} - \frac{3}{r^2}\varphi_{2rr}^{(1)} + \frac{3}{r^3}\varphi_{2r}^{(1)}\right)\\
&\quad = \mathrm{i}\alpha_c\left[\frac{1}{r}(\varphi_1\varphi_{1rrr}^* - \varphi_1^*\varphi_{1rrr}) - \frac{3}{r^2}(\varphi_1\varphi_{1rr}^* - \varphi_1^*\varphi_{1rr})\right.\\
&\qquad \left. + \frac{3}{r^3}(\varphi_1\varphi_{1r}^* - \varphi_1^*\varphi_{1r}) + \frac{1}{r}(\varphi_{1r}\varphi_{1rr}^* - \varphi_{1r}^*\varphi_{1rr})\right]\\
&\qquad + \frac{1}{Re_c}\left(-rW''' - W'' + \frac{W'}{r}\right) \qquad (59)
\end{aligned}$$

with the boundary conditions

$$\varphi_2^{(1)}(0) = 0, \quad \varphi_2^{(1)}(1) = 0, \quad \varphi_{2r}^{(1)}(0) = 0, \quad \varphi_{2r}^{(1)}(1) = 0. \quad (60)$$

Finally, collecting the terms that are proportional to $A_\xi \exp[ik_c(x-ct)]$ gives

$$
\begin{aligned}
&i\alpha_c(W-c_c)\left(\varphi_{2rr}^{(2)}-\frac{\varphi_{2r}^{(2)}}{r}-\alpha_c^2\varphi_2^{(2)}\right)+i\alpha_c\varphi_2^{(2)}\left(-W''+\frac{W'}{r}\right)\\
&\quad+\frac{1}{Re_c}\left(-\varphi_{2rrrr}^{(2)}+\frac{2}{r}\varphi_{2rrr}^{(2)}-\frac{3}{r^2}\varphi_{2rr}^{(2)}+2\alpha_c^2\varphi_{2rr}^{(2)}+\frac{3}{r^3}\varphi_{2r}^{(2)}-\frac{2\alpha_c^2}{r}\varphi_{2r}^{(2)}-\alpha_c^4\varphi_2^{(2)}\right)\\
&=c_g\left(\varphi_{1rr}-\frac{\varphi_{1r}}{r}-\alpha_c^2\varphi_1\right)+\varphi_1\left(W''-\frac{W'}{r}+3\alpha_c^2W-2\alpha_c^2c_c\right)+W\frac{\varphi_{1r}}{r}\\
&\quad-W\varphi_{1rr}+\frac{4i\alpha_c}{Re_c}\left(\varphi_{1rr}-\frac{\varphi_{1r}}{r}-\alpha_c^2\varphi_1\right)
\end{aligned}
\tag{61}
$$

with the boundary conditions

$$
\varphi_2^{(2)}(0)=0,\quad \varphi_2^{(2)}(1)=0,\quad \varphi_{2r}^{(2)}(0)=0,\quad \varphi_{2r}^{(2)}(1)=0. \tag{62}
$$

The function $\varphi_2^{(2)}(r)$ in (61), (62) is resonantly forced since the corresponding homogeneous problem is satisfied with $\alpha=\alpha_c$, $c=c_c$ and $Re=Re_c$. Therefore, problem (61), (62) has a solution if and only if the right-hand side of (61) is orthogonal to the adjoint function $\varphi_1^a(r)$. The adjoint operator, L_1^a, and the adjoint function, $\varphi_1^a(r)$, to the linear operator L_1 are defined as follows:

$$
\int_0^1 \varphi_1^a\, L_1[\varphi_1]\,dr=\int_0^1 \varphi_1\, L_1^a[\varphi_1^a]\,dr=0, \tag{63}
$$

where

$$
\begin{aligned}
L_1^a[\varphi_1^a]&=\varphi_{1rrrr}^a+\frac{2}{r}\varphi_{1rrr}^a-\left(\frac{3}{r^2}+2\alpha_c^2+i\alpha_cRe_cW\right)\varphi_{1rr}^a\\
&\quad+\left(\frac{3}{r^3}-\frac{2\alpha_c^2}{r}-2i\alpha_cRe_cW'-\frac{i\alpha_cRe_cW}{r}\right)\varphi_{1r}^a\\
&\quad+\left(-\frac{3}{r^4}+\frac{2\alpha_c^2}{r^2}-\frac{2i\alpha_cRe_cW'}{r}+\frac{i\alpha_cRe_cW}{r^2}+i\alpha_c^3Re_cW+\alpha_c^4\right)\varphi_1^a\\
&\quad+i\alpha_cRe_c\left[\varphi_{1rr}^a+\frac{\varphi_{1r}^a}{r}-\left(\alpha_c^2+\frac{1}{r^2}\right)\varphi_1^a\right].
\end{aligned}
\tag{64}
$$

The boundary conditions are

$$
\varphi_1^a(0)=0,\quad \varphi_1^a(1)=0,\quad \varphi_{1r}^a(0)=0,\quad \varphi_{1r}^a(1)=0. \tag{65}
$$

Integrating the left-hand side of equation (63) by parts and using boundary conditions (48), (65) we obtain the adjoint operator $L_1^a[\varphi_1^a]$. The parameters α_c and Re_c in (64), (65) are the critical values obtained from the solution of the linear stability problem (46), (48). The adjoint operator L_1^a must have the same spectrum as the linear operator L_1. Our calculations confirm that this is the case. The solvability condition for problem (61), (62) gives the value of c_g which has to be real. Using third-order accuracy, the group velocity c_g was evaluated for several parameter sets. These calculations reveal that c_g is real. For example, for Case III and with $\tilde{t}=2.8$ s, $\alpha_c=3.6949$, $Re_c=499.3265$, $c_c=0.0326$ and $c_g=-0.0651$.

The equation for the amplitude of A is obtained from the solvability condition for equation (55). Substituting (52) and (56) into the right-hand side of (55), multiplying the resulting expression by φ_1^a, integrating it with respect to r from 0 to 1 and using the solvability condition, we obtain the following complex Ginzburg–Landau equation for the amplitude $A(\xi, \tau)$:

$$A_\tau = \sigma A + dA_{\xi\xi} - \mu A|A|^2, \tag{66}$$

where the complex coefficients σ, d and μ are given by

$$\sigma = \frac{\sigma_1}{b}, \quad d = \frac{d_1}{b}, \quad \mu = \frac{\mu_1}{b}. \tag{67}$$

The constants b, σ_1, d_1 and μ_1 are defined as follows:

$$b = \int_0^1 \varphi_1^a \left(\varphi_{1rr} - \frac{\varphi_{1r}}{r} - \alpha_c^2 \varphi_1\right) \mathrm{d}r, \tag{68}$$

$$\sigma_1 = -\frac{1}{Re_c} \int_0^1 \varphi_1^a \left[\varphi_{1rrrr} - \frac{2}{r}\varphi_{1rrr} + \left(\frac{3}{r^2} - 2\alpha_c^2\right)\varphi_{1rr} + \left(\frac{2\alpha_c^2}{r} - \frac{3}{r^3}\right)\varphi_{1r} + \alpha_c^4 \varphi_1\right] \mathrm{d}r, \tag{69}$$

$$\begin{aligned} d_1 = \int_0^1 \varphi_1^a \Bigg\{ & \varphi_{2rr}^{(2)} \left[c_g - W + \frac{4\mathrm{i}\alpha_c}{Re_c}\right] + \varphi_{2r}^{(2)} \left[\frac{W - c_g}{r} - \frac{4\mathrm{i}\alpha_c}{rRe_c}\right] \\ & + \varphi_2^{(2)} \left(-c_g \alpha_c^2 - 2\alpha_c^2 c_c + W'' - \frac{W'}{r} + 3\alpha_c^2 W - \frac{4\mathrm{i}\alpha_c^3}{Re_c}\right) \\ & + \varphi_1 \left(2\mathrm{i}\alpha_c c_g + \mathrm{i}\alpha_c c_c - 3\mathrm{i}\alpha_c W - \frac{6\alpha_c^2}{Re_c}\right) + \frac{2}{Re_c}\varphi_{1rr} - \frac{2}{rRe_c}\varphi_{1r} \Bigg\} \mathrm{d}r, \end{aligned} \tag{70}$$

$$\begin{aligned} \mu_1 = -\int_0^1 \varphi_1^a \Bigg\{ & \frac{3\mathrm{i}\alpha_c}{r^3}(\varphi_1 \varphi_{2r}^{(1)} - \varphi_1^* \varphi_{2r}^{(0)} + 2\varphi_2^{(0)} \varphi_{1r}^*) \\ & + \frac{\mathrm{i}\alpha_c}{r^2}(-6\varphi_2^{(0)} \varphi_{1rr}^* - 3\varphi_1 \varphi_{2rr}^{(1)} + 3\varphi_1^* \varphi_{2rr}^{(0)} - 4\alpha_c^2 \varphi_2^{(0)} \varphi_1^* + \varphi_{1r}^* \varphi_{2r}^{(0)} + \varphi_{1r} \varphi_{2r}^{(1)}) \\ & + \frac{\mathrm{i}\alpha_c}{r}(2\varphi_2^{(0)} \varphi_{1rrr}^* - \varphi_1^* \varphi_{2rrr}^{(0)} + \varphi_1 \varphi_{2rrr}^{(1)} + \varphi_{2r}^{(0)} \varphi_{1rr}^* - \varphi_{2r}^{(1)} \varphi_{1rr} - 2\varphi_{1r}^* \varphi_{2rr}^{(0)} \\ & - 2\alpha_c^2 \varphi_2^{(0)} \varphi_{1r}^* + 3\alpha_c^2 \varphi_1^* \varphi_{2r}^{(0)} + \alpha_c^2 \varphi_1 \varphi_{2r}^{(1)} + 8\alpha_c^2 \varphi_{1r}^* \varphi_2^{(0)}) \Bigg\} \mathrm{d}r. \end{aligned} \tag{71}$$

Note that Wu (1993), Wu, Lee & Cowley (1993) and Wu & Cowley (1995) showed, unlike the present *ad-hoc* approach, the self-consistent approach of Cowley (1987) does not lead to an equation of the Ginzburg–Landau type. Instead, integro-differential equations with history-dependent nonlinear terms arise. In addition, the form of the amplitude equation also depends on whether the mode is two-dimensional or three-dimensional.

5.2. *Numerical results and discussion*

In order to calculate the coefficients of the Ginzburg–Landau equation one needs to solve the boundary value problems (57)–(62) numerically. The solution is found by

Case	$\tilde{t}_p$ (s)	α_c	Re_c	c_c	σ	μ
III	2.8	3.6949	499.3265	0.0326	0.2338 + 0.0767i	2164.4 + 3646.7i
IV	1.8	4.1501	1120.0861	0.0121	0.1081 + 0.0250i	7235.5 + 8579.6i

TABLE 4. Values of the coefficients of equation (73) for Cases III and IV.

the Chebyshev collocation method where the functions $\varphi_2^{(i)}(r)$ are sought in the form

$$\varphi_2^{(i)}(r) = \sum_{m=0}^{M} a_m^{(i)}(1-x^2)^2 T_m(x), \tag{72}$$

where $a_m^{(i)}$ are unknown complex coefficients. The variable x is related to r by the formula $x = 2r - 1$. The collocation points are $x_j = \cos \pi j/M$, $j = 0, 1, \ldots, M$. The form (72) guarantees that the boundary conditions for the functions $\varphi_2^{(i)})(r)$ are automatically satisfied.

The complex Ginzburg–Landau equation (66) can have a great variety of solutions depending on the values of its coefficients (Cross & Hohenberg 1993). The existence of finite-equilibrium solutions depends on the sign of the real part of the constant μ in (66) (known as the Landau constant in the hydrodynamic stability literature). If one neglects the dependence of A on ξ, then (66) reduces to the following nonlinear ODE known as the Landau equation:

$$A_\tau = \sigma A - \mu A|A|^2. \tag{73}$$

The coefficients of the Landau equation are calculated for two sets of experimental conditions in DA (Case III and Case IV) for which the most unstable mode is the axisymmetric mode with $n = 0$. Therefore, the weakly nonlinear theory developed in this section is applicable for these two cases. The starting point for a weakly nonlinear analysis is the critical Reynolds number Re_c and the corresponding critical values α_c and c_c. Since the base flow is time-dependent, it is not clear in advance which value of time to select in order to calculate Re_c, α_c and c_c. It follows from table 1 that the experimentally observed time $\tilde{t}_p$ at which the instability sets in is around $\tilde{t}_p = 2.8$ s for Case III and $\tilde{t}_p = 1.8$ s for Case IV. These values are also chosen for our calculations. However, we also calculated the values of the coefficients of equation (73) for other values of time in the interval $(\tilde{t}_2, \tilde{t}_p)$. The conclusion is that the sign of the real part of the Landau constant does not change in these intervals. The values of the coefficients of equation (73) for Case III and Case IV are summarized in table 4.

As can be seen from table 4, the real part of the Landau constant is positive in both cases. Hence, finite-amplitude equilibrium is possible. Note that flow visualization in Case III in DA showed a secondary vortex induced by the primary vortex. The growth of secondary vortices finally led to turbulence. In Case IV, however, the breakdown to turbulence does not occur. The vortices remain near the wall and move in the horizontal direction. These experimental findings are, at least qualitatively, confirmed by weakly nonlinear theory.

6. Conclusions

Some aspects of unsteady flows in pipes are considered in the present paper. An asymptotic solution for a laminar axisymmetric unidirectional flow in a pipe subject to acceleration or deceleration is derived by the method of matched asymptotic ex-

pansions. The flow before acceleration or deceleration can be steady or unsteady (but unidirectional). Excellent agreement for small times is found between the asymptotic solution and analytical solution for the case of sudden closure of the pipe.

Since velocity profiles during the deceleration phase have inflection points, these profiles are potentially unstable. Therefore a linear stability analysis of time-dependent flow in a pipe is carried out. The results of calculations are compared with experimental data in DA where the flow is generated by the motion of a piston which was linearly accelerated over the interval $(0, \tilde{t}_0)$, maintained at constant velocity in the interval $(\tilde{t}_0, \tilde{t}_1)$ and decelerated to zero over the time $(\tilde{t}_1, \tilde{t}_2)$. Stability characteristics are calculated for different values of the parameters $\tilde{t}_0$, $\tilde{t}_1$ and $\tilde{t}_2$. The use of a quasi-steady assumption allows one to explain many of the experimental results obtained by DA. Moreover, the planar flow assumption used by DA in their paper is relaxed and full three-dimensional perturbations are studied in the framework of linear stability theory. It is shown that the planar flow assumption works well for a boundary layer type of flow. If the flow is more developed (for example, if $\tilde{t}_1$ is sufficiently large), then the planar flow assumption gives only qualitatively good results. It is found that for large values of $\tilde{t}_1$ the growth rates are considerably overestimated by the planar flow assumption. Moreover, the error in determining the critical Reynolds numbers can be as large as 60%. Numerical predictions show satisfactory agreement with experimental data presented in DA.

An amplitude evolution equation for the case of linearly unstable axisymmetric perturbations is derived by means of weakly nonlinear theory. The coefficients of the Landau equation are calculated for two cases reported in experiments of DA (namely, Case III and Case IV). Calculations show that the axisymmetric mode is the most unstable mode for these two cases. It is found that the real part of the Landau constant is positive in both cases. Hence, the instability is supercritical and finite-amplitude equilibrium is possible. These results are qualitatively supported by experiments in DA where the secondary flows are found by a flow visualization technique.

The authors gratefully acknowledge the financial support of this work by the Hong Kong Research Grant Council (HKUST6092/00E).

REFERENCES

Allmen, M. J. & Eagles, P. M. 1984 Stability of divergent channel flows: a numerical approach. *Proc. R. Soc. Lond.* A **392**, 359–372.

Akhavan, R., Kamm, R. D. & Shapiro, A. H. 1991 An investigation of transition to turbulence in bounded oscillatory Stokes flows. Part 2. Numerical simulations. *J. Fluid Mech.* **225**, 423–444.

Batchelor, G. K. & Gill, A. E. 1962 Analysis of the stability of axisymmetric jets. *J. Fluid. Mech.* **14**, 529–551.

Brunone, B., Karney, B., Mecarelli, M. & Ferrante, M. 2000 Velocity profiles and unsteady pipe friction in transient flow. *J. Water Resourc. Planning Management* **126**, 236–244.

Cowley, S. J. 1987 High frequency Rayleigh instability of Stokes layers. In *Stability of Time Dependent and Spatially Varying Flows* (ed. D. L. Dwoyer & M. Y. Hussaini), pp. 261–275.

Cross, M. C. & Hohenberg, P. C. 1993 Pattern formation outside of equilibrium. *Rev. Mod. Phys.* **65**, 851–1112.

Davis, S. H. 1976 The stability of time-periodic flows. *Annu. Rev. Fluid Mech.* **8**, 57–74.

Das, D. & Arakeri, J. H. 1998 Transition of unsteady velocity profiles with reverse flow. *J. Fluid Mech.* **374**, 251–283 (referred to herein as DA).

Davey, A. & Nguyen, H. P. F. 1971 Finite-amplitude stability of pipe flow. *J. Fluid Mech.* **45**, 701–720.

Drazin, P. & Reid, W. 1981 *Hydrodynamic Stability*. Cambridge University Press.

Gad-el-Hak, M., Davis, S. H., McMurray, J. T. & Orszag, S. A. 1984 On the stability of decelerating laminar boundary layer. *J. Fluid Mech.* **138**, 297–323.

Garg, V. K. 1981 Stability of developing flow in a pipe: non-axisymmetric disturbances. *J. Fluid Mech.* **110**, 209–216.

Ghidaoui, M. S. & Kolyshkin, A. A. 2001 Stability analysis of velocity profiles in water-hammer flows. *J. Hydraul. Engng* **127**, 499–512.

Gromeka, I. S. 1882 On the theory of fluid motion in narrow cylindrical pipes. *Kazan University Research Notes*, 32 pp. (In Russian).

Hall, P. & Parker, K. H. 1976 The stability of the decaying flow in a suddenly blocked channel flow. *J. Fluid Mech.* **75**, 305–314.

Hino, M., Sawamoto, M. & Takasu, S. 1976 Experiments in transition to turbulence in an oscillatory pipe flow. *J. Fluid Mech.* **75**, 193–207.

Holomboe, E. L. & d Roleau, W. T. 1967 The effect of viscous shear on transients in liquid lines. *Trans. ASME: J. Basic Engng* **89**, 174–180.

von Kerczek, C. & Davis, S. H. 1974 Linear stability theory of oscillatory Stokes layers. *J. Fluid Mech.* **62**, 753–773.

Kevorkian, J. & Cole, J. D. 1996 *Multiple Scale and Singular Perturbation Methods*. Springer.

Khorrami, M. R., Malik, M. R. & Ash, R. L. 1989 Application of spectral collocation techniques to the stability of swirling flows. *J. Comput. Phys.* **81**, 206–229.

Krane, M. J. M. & Gebhart, B. 1993 The hydrodynamic stability of a one-dimensional transient buoyancy-induced flow. *Intl J. Heat Mass Transfer* **36**, 977–988.

Moss, E. A. & da Silva, D. F. 1993 The evolution of unstable regions in impulsively started pipe entrance flows. *Phys. Fluids* A **5**, 2721–2724.

Ramaprian, B. R. & Mueller, A. 1980 Transitional periodic boundary layer study. *J. Hydraul. Div., ASCE* **106**, 1959–1971.

Sarpkaya, T. 1993 Coherent structures in oscillatory boundary layer. *J. Fluid Mech.* **253**, 105–140.

Shen, S. F. 1961 Some considerations on the laminar stability of time-dependent basic flows. *J. Aero. Sci.* **28**, 397–404.

da Silva, D. F. & Moss, E. A. 1994 The stability of pipe entrance flows subjected to axisymmetric disturbances. *Trans. ASME: J. Fluids Engng* **116**, 61–65.

Stewartson, K. & Stuart, J. T. 1971 A nonlinear instability theory for a wave system in plane Poiseuille flow. *J. Fluid. Mech.* **48**, 529–545.

Stuart, J. T. 1960 On the nonlinear mechanics of wave disturbances in stable and unstable parallel flows. Part 1. The basic behaviour in plane Poiseuille flow. *J. Fluid. Mech.* **9**, 353–370.

Telionis, D. P. 1981 *Unsteady Viscous Flows*. Springer.

Waters, S. L. & Pedley, T. J. 1999 Oscillatory flow in a tube of time-dependent curvature. Part 1. Perturbation to flow in a stationary curved tube. *J. Fluid Mech.* **383**, 327–352.

Weinbaum, S. & Parker, K. H. 1975 The laminar decay of suddenly blocked channel and pipe flows. *J. Fluid Mech.* **69**, 729–752.

Wu, X. 1993 Nonlinear temporal-spatial modulation of near-planar Rayleigh waves in shear flows: formation of streamwise vortices. *J. Fluid. Mech.* **256**, 685–719.

Wu, X., Lee, S. S. & Cowley, S. J. 1993 On the weakly nonlinear three-dimensional instability of shear layers to pairs of oblique waves: the Stokes layer as a paradigm. *J. Fluid. Mech.* **253**, 681–721.

Wu, X. & Cowley, S. J. 1995 On the nonlinear evolution of instability modes in unsteady shear layers: the Stokes layer as a paradigm. *Q. J. Mech. Appl. Maths* **48**, 159–188.

Wylie, E. B. & Streeter, V. L. 1993 *Fluid Transient in Systems*. Prentice-Hall.

Yang, K. S., Spalart, P. R. & Ferziger, J. H. 1992 Numerical studies of natural transition in a decelerating boundary layer. *J. Fluid Mech.* **240**, 433–468.

Yang, W. H. & Yih, C.-S. 1977 Stability of time-periodic flows in a circular pipe. *J. Fluid Mech.* **82**, 497–505.